Differential modifications of the C-terminal tails of α-tubulin isoforms and their importance for kinesin-based microtubule transport *in vivo*

Mengjing Bao, Ruth Dörig, Dirk Beuchle, Paula Maria Vazquez-Pianzola and Beat Suter

Institute of Cell Biology, University of Bern, Switzerland

Summary

1. α-tubulin glutamylation was identified specifically on the C-terminal domain of TBA1 and TBA3 (TBA1/3). Multiple glutamyl residues were pinpointed on these isoforms. The *Drosophila* female germline isoform TBA4 is not glutamylated.
2. *TTLL5* is required for mono- and polyglutamylation of TBA1/3.
3. Glutamylation of α-tubulin is required for proper kinesin-based localization of Staufen/*osk* mRNA, ooplasmic streaming during oogenesis, and kinesin-based transport of mitochondria in neurons.

Abstract

Microtubules (MTs) are built from α-/β-tubulin dimers and used as tracks by kinesin and dynein motors to transport a variety of cargos, such as mRNAs, proteins, and organelles, within the cell. Tubulins are subjected to several post-translational modifications (PTMs). Glutamylation is one of them, and it is responsible for adding one or more glutamic acid residues as branched peptide chains to the C-terminal tails of both α- and β-tubulin. However, very little is known about the specific modifications found on the different tubulin isoforms *in vivo* and the role of these PTMs in cargo transport along MTs *in vivo*. In this study, we found that in *Drosophila*, glutamylation of the α-tubulin isoforms occurs specifically on the C-terminal ends of TBA1 and TBA3 in the ovaries. In contrast, the ovarian isoform TBA4 is not glutamylated. The C-terminal ends of TBA1 and TBA3 are glutamylated at several glutamyl side chains in various combinations. *Drosophila TTLL5* is required for the mono- and polyglutamylation of ovarian TBA1 and 3. Furthermore, glutamylation of the α-tubulin is essential for the efficient localization of Staufen/*osk* mRNA and to give directionality to the fast ooplasmic streaming, two processes known to depend on kinesin-mediated processes during oogenesis. In the nervous system, the kinesin-dependent

neuronal transport of mitochondria also depends on *TTLL5*. Additionally, α-tubulin glutamylation affects the pausing of the transport of individual mitochondria in the axons. Our results demonstrate the *in vivo* role of *TTLL5* in differential glutamylation of α-tubulin isoforms and point to the *in vivo* importance of α-tubulin glutamylation for kinesin-dependent processes.

Introduction

Microtubules (MTs) are fundamental cytoskeletal filaments comprising heterodimers of α- and β-tubulins. Despite the high level of conservation in eukaryotes, MTs are still quite diverse because cells express different isoforms, and these can undergo several different post-translational modifications (PTMs). Based mainly on *in vitro* assays, these isoform variations are thought to optimize the MT interaction with different microtubule-associated proteins (MAPs) and motors.

Drosophila melanogaster possesses four α-tubulin genes. Three of them are expressed during oogenesis and early embryogenesis, suggesting that they contribute to the formation of microtubules during these stages. The three genes are *αTub84B*, *αTub84D,* and *αTub67C* (Kalfayan and Wensink, 1982). *αTub84B* and *αTub84D* encode the TBA1 and TBA3 isoforms of α-tubulin, respectively, which differ in only two amino acids. Their primary sequence in the C-terminal domain is identical, and both are expressed in most tissues and throughout development. In contrast, *αTub67C* encodes TBA4 and is expressed exclusively during oogenesis, where it is maternally loaded into the egg and embryo. The primary structure of TBA4 is distinctively different from TBA1/3 (Theurkauf et al., 1986). These differences are also apparent in the C-terminal domain and include the last residue, which is phenylalanine (Phe, F) in TBA4 and tyrosine (Tyr, Y) in TBA1/3. *αTub85E,* which encodes TBA2, is mainly expressed in testes (Kalfayan and Wensink, 1982).

MTs are subjected to several PTMs, including the C-terminal tail glutamylation, glycylation, and detyrosination / tyrosination (Arce et al., 1975, Eddé et al., 1990, Redeker et al., 1994, Hallak et al., 1977). Furthermore, acetylation and phosphorylation in the more central parts of the tubulins have also been identified (Arce et al., 1975; Eddé et al., 1990; Hallak et al., 1977; L'Hernault and Rosenbaum, 1985; Magiera and Janke, 2014; Redeker et al., 1994). Glutamylation is a PTM that adds one or more glutamic acids (Glu, E) to the side chains of glutamic acid residues in the C-terminal tails of both α and β tubulin, causing the formation of a branched peptide chain (Eddé et al., 1990; Redeker et al., 1992). Glycylation is another PTM that adds glycines to the γ-carboxyl group of glutamic acid residues in the C-terminal region (Redeker et al., 1994). At least in vertebrates, tubulin is also subjected to a particular cycle of de-tyrosination-tyrosination (Preston et al., 1979). In this case, the C-terminal Tyr or Phe of α-tubulin is cyclically removed, resulting in a C-terminal Glu residue, and a new Tyr can be re-added to the new C-term. The enzymes that catalyze glutamylation, glycylation, and tyrosination belong to the Tubulin-tyrosine-ligase-like (TTLL) family (Janke et al., 2005). In *Drosophila melanogaster*, this family encompasses 11 genes (flybase.org).

74 *CG31108* is considered the homolog of the mammalian *TTLL5* gene and was therefore
75 named *DmTTLL5 or TTLL5* (Devambez et al., 2017). It is required for α-tubulin glutamylation
76 in the *Drosophila* nervous system (Devambez et al., 2017). The murine TTLL5 is composed
77 of an N-terminal core tubulin tyrosination ligase-like (TTLL) domain, a cofactor interaction
78 domain (CID), and a C-terminal receptor interaction domain (RID) (Lee et al., 2013). The N-
79 terminal core domain was shown to provide the catalytic activity of TTLL5 and is highly
80 conserved in *Drosophila* TTLL5 (van Dijk et al., 2007) (**Table 1**). According to the FlyBase
81 data, *Drosophila TTLL5* mRNA is expressed at high levels in ovaries (**Table S2**), even
82 higher than in the nervous system where initial studies were performed (Devambez et al.,
83 2017). We thus focused on *TTLL5*'s possible functions during *Drosophila* oogenesis to shed
84 light on possible *in vivo* roles of glutamylated α-tubulins.

85 MTs have an intrinsic polarity with a plus and a minus end. On these tracks, kinesin
86 motors transport cargo to the plus ends, and dynein motors move cargo towards the minus
87 ends. Evidence for the importance of PTMs of tubulin subunits has already been reported *in*
88 *vitro.* Artificial tethering of 10E peptides to the side chains at position E445 of α-tubulin and
89 E435 of β-tubulin by maleimide chemistry increased the processivity (the run length) of
90 kinesin motors on tubulin. For Kinesin-1, this was a 1.5-fold increase (Sirajuddin et al.,
91 2014). In contrast to Kinesin, Dynein/dynactin motors preferred a Tyr at the C-term of α-
92 tubulin to initiate processive transport *in vitro*, because the motor favored this isoform as an
93 attachment point to dock onto the MTs (McKenney et al., 2016). Recent work now also
94 demonstrated a role for the mouse tubulin glycylation enzymes. *In vitro* fertility assays
95 showed that the lack of both *TTLL3* and *TTLL8* perturbed sperm motility, causing male
96 subfertility in mice. Structural analyses further suggested that loss of glycylation decreased
97 axonemal dynein activity (Gadadhar et al., 2021).

98 A recent *in vivo* mouse study showed that hyperglutamylation of α-tubulin by TTLL1, but
99 not β-tubulin, increased the overall (both anterograde and retrograde) motility of
100 mitochondria, perturbed axonal transport, and led to neurodegeneration (Bodakuntla et al.,
101 2021). Surprisingly, however, another study showed that the vesicular axonal transport was
102 not affected by the absence of MT glutamylation in *Drosophila TTLL5* mutant larvae
103 (Devambez et al., 2017). Given these results and because the *Drosophila* gene is also highly
104 expressed in ovaries, we studied the *in vivo* role of *TTLL5* with a particular focus on the
105 PTMs of the different α-tubulin isoforms in the ovary. This revealed that *TTLL5* is essential
106 for the normal glutamylation of the standard TBA1 and three isoforms. Surprisingly, even in
107 wild-type ovaries, the oogenesis-specific TBA4 was not glutamylated, suggesting that this
108 isoform may have evolved to produce MTs that contain regions that cannot be glutamylated.
109 We also found that *TTLL5* is required *in vivo* for the localization of mRNAs and cytoplasmic

streaming, suggesting that these activities indeed depend on polyglutamylation of α-tubulin. The transport of mitochondria in wing nerves is another attractive system to study organelle transport (Vagnoni and Bullock, 2016) (Hollenbeck and Saxton, 2005). We found that the initiation of axonal transport of mitochondria in wing nerves was strongly affected by the lack of *TTLL5*. The overall motility and the processivity of the mitochondrial transport also appeared to depend on α-tubulin glutamylation. Our work, therefore, reveals the *in vivo* importance of glutamylation of specific α-tubulin isoforms.

118 **Results**

119 **Specific glutamylation on multiple Glu residues in TBA1/3, but not TBA4 in ovaries**

120 Mass spectrometry experiments were initially performed to analyze the glutamylation of the
121 C-terminal tails of α-tubulins *in vivo*. Proteins extracted from ovaries were purified through
122 SDS-PAGE, and α-tubulin bands were cut out and digested with the protease trypsin-N. C-
123 terminal peptides of the different α-tubulin isoforms were then analyzed for post-translational
124 modifications by liquid chromatography-mass spectrometry (LC-MS). Because the resulting
125 C-terminal peptides are identical between the TBA1 and TBA3 isoforms, we refer to them as
126 TBA1/3 (**Fig. 1A**). Analyses of wild-type ovarian extracts revealed that the general
127 *Drosophila* isoforms TBA1/3, but not the ovarian-specific TBA4 isoform of α-tubulin, showed
128 glutamylation on the C-terminal tail of α-tubulins (**Fig. 1A**, **S1**). For TBA1/3, side chain
129 glutamylation was identified on all four glutamyl residues in the tail region, Glu443, Glu445,
130 Glu448, and Glu449, and the longest side chains identified consisted of 3Es in wild-type
131 ovaries **(Fig. 1A,1B).**

132

133 ***Drosophila TTLL5* is required for MT mono- and polyglutamylation of ovarian TBA1/3**

134 To study the function of TTLL5, distinct *TTLL5* loss-of-function mutations were created and
135 characterized (**Fig. 2A**). The $TTLL5^{pBac}$ and $TTLL5^{Mi}$ mutant strains carry a piggyBac and a
136 Minos transposon, respectively, within the open reading frame of *TTLL5*. The $TTLL5^{MiEx}$
137 mutant was generated by imprecise excision of the Minos element, which caused the
138 formation of a premature stop codon at gene position 8,132 in the open reading frame
139 (codon position 392). An anti-TTLL5 antibody that cross-reacts with additional proteins in
140 ovarian extracts also recognized a band corresponding to the mass of TTLL5. This band was
141 absent in ovarian extracts prepared from the three *TTLL5* mutants, suggesting that they are
142 protein nulls for *TTLL5* or make only a truncated protein (**Fig. 2B**). A transgene containing
143 the wild-type *Drosophila TTLL5* sequence fused to the Venus fluorescent protein sequence
144 under UAS control (UASP-*Venus::TTLL5*) was also produced as a tool to rescue the
145 phenotypes produced by the *TTLL5* mutations and for overexpression studies (**Fig. 2A**).

146 To quantify the effect of *TTLL5* on the glutamylation of the C-terminal tails of α-tubulins,
147 we determined the frequency of C-terminal peptides containing the entire primary sequence
148 and 0, 1, 2, and 3 Glu (E) modifications. This analysis was performed with extracts from wild-
149 type ovaries and the different *TTLL5* mutant ovaries. Wild-type ovaries revealed that 62% of
150 the peptides were modified, 41% with 1E, 14% with 2Es, and 7% with 3Es **(Table 1)**. On the

151 other hand, no glutamylation was observed in *TTLL5*^{pBac} and *TTLL5*^{MiEx} mutants. This clearly
152 shows that *Drosophila TTLL5* is essential for the side chain glutamylation of the C-terminal
153 Glu443, Glu445, Glu448, and Glu449 of TBA1/3.

154 We also measured the levels of monoglutamylation of α-tubulin by Western blotting using
155 the GT335 antibody. This antibody reacts with the first glutamate on the glutamate side-
156 chain even if it is polygutamylated (**Fig. 3A**) (Wolff et al., 1992). Note that the GT335
157 antibody does not reliably detect all mono glutamylated residues in *Drosophila* tubulins
158 because GT335 preferentially recognizes the first Glu attached to a Glu residue in an acidic
159 environment. In mice, the middle Glu in the sequence -G**E**E- of the C-terminal tail of α-
160 tubulin is such an "acidic" site. Once glutamylated, the branched Glu modification can be
161 recognized by GT335 (Bodakuntla et al., 2021). In contrast, in *Drosophila* α-tubulin, both
162 E443 and E445 in the sequence -G**E**G**E**G- are flanked by Glycines on both sides, which
163 does not provide the acidic environment needed for efficient recognition by GT335. The
164 GT335 signal may, therefore, mainly stem from the glutamylation on the consecutive Glu
165 residues E448 and E449 in the sequence -GA**EE**Y. On Western blots from wild-type
166 extracts, the GT335 antibody produced a band at the expected position, and this band was
167 reduced in all *TTLL5* mutants. The GT335 signals were restored and even increased in
168 some *TTLL5* mutants upon overexpression of the rescue construct *Venus::TTLL5*, showing
169 that the signal is specific and can be used to monitor *TTLL5* activity **(Fig. 3B)**. We conclude
170 that *TTLL5* is required for monoglutamylation of α-tubulin.

171 The 1D5 antibody recognizes α-tubulin with an -XEE sequence at the C-terminal α-
172 carboxylate group (with X being a variable residue) (Rüdiger et al., 1999) **(Fig. 3A')**.
173 Therefore, in principle, all the Glu residues on E443, E445, E448 E449, and the C-terminal
174 Glu residues E448/449 can be recognized if they are not followed by another amino acid
175 (such as Tyr) at the α-carboxylate group. 1D5 does not cross-react with C-terminal Glu
176 residues E448/449 in tyrosinated α-tubulin. Because *w* control ovaries showed high 1D5
177 cross-reactivity with a polypeptide of the predicted size, this, therefore, indicates the
178 presence of glutamate side chains containing at least two glutamates and possibly de-
179 tyrosinated isoforms of α-tubulin (Gadadhar et al., 2017; Preston et al., 1979) **(Fig. 3B',**
180 **3B'')**. Consistent with the MS analysis, the *TTLL5* mutants showed a strongly reduced signal
181 with 1D5, indicating that loss of *TTLL5* function prevents normal polyglutamylation. The 1D5
182 signal was again restored in all *TTLL5* mutants upon expression of the rescue construct.
183 Overexpression of TTLL5 in *TTLL5*^{pBac} and *TTLL5*^{Mi} even produced a stronger 1D5 signal
184 and an up-shifted band, suggesting that α-tubulin gets hyper-glutamylated, maybe on
185 additional sites **(Fig. 3B')**. We also tested whether the overexpression of *TTLL5* in a wild-

186 type background affected polyglutamylation similarly. Indeed, *UASP-Venus::TTLL5*
187 overexpression in ovaries led to hyper glutamylation, as evident from the stronger signal and
188 the additional upshifted band **(Fig. 3C).** Glutamylation of β-tubulin was also evaluated by
189 using the antibody β-monoE, which specifically recognizes monoglutamylation of the C-
190 terminal tail of β-tubulin (Bodakuntla et al., 2021) **(Fig. 3B").** The results showed a strong
191 signal of β-monoE in control ovaries, indicating that monoglutamylation occurred on β-tubulin
192 in ovaries. However, the β-monoE levels were kept unchanged whether *TTLL5* was
193 overexpressed or mutated. These results reveal that *TTLL5* is essential for the glutamylation
194 of MTs in the ovary, acting specifically on α-tubulin but not on the β- tubulin subunit. It also
195 suggests that TTLL5 levels are usually limiting in ovaries.

196 Most of the murine TTLL5 residues involved in α-tubulin glutamylation (van Dijk et al.,
197 2007) are conserved in *Drosophila* TTLL5 **(Table 2)**. Two are known to be essential for the
198 general enzymatic activity of TTLLs, and two for the interaction with the C-terminal domain of
199 α-tubulin **(Fig. 3D)**. To determine whether these residues are indeed needed *in vivo* for the
200 enzymatic activity of *Drosophila TTLL5 towards* TBA1/3, we used CRISPR/Cas9 to mutate
201 the conserved codons in *Drosophila TTLL5. Drosophila* TTLL5 residues K282 and E517
202 correspond to mouse K131 and E336*,* respectively*.* They directly interact with ADP/ATP and
203 thus affect general TTLL5 enzymatic activity (van Dijk et al., 2007). TTLL5^{R339} corresponds
204 to mouse TTLL5^{R188}*,* which is vital for TTLL5's glutamylation activity. MmTTLL5^{R188} resides in
205 the β6-7 loop, which forms a salt-bridge interaction with the C-terminal tail of α-tubulin and
206 orients it towards the ATP/ADP-binding site (van Dijk et al., 2007). Glutamylation of α-tubulin
207 was impaired in all these *TTLL5* mutants where the conserved residue was replaced **(Fig.**
208 **3E)**. Since these mutations did not abolish the stability of the corresponding mutant protein
209 (**Fig. S2**), our results revealed the importance of E517, K282, and R399 of *Drosophila* TTLL5
210 for glutamylation. Most active site residues of human TTL (Prota et al., 2013; van Dijk et al.,
211 2007) are also conserved between mammalian and *Drosophila* TTLL5 **(Table 3)**. We also
212 mutated the *Drosophila TTLL5^{P522}* codon corresponding to human *TTL^{P336}* (and mouse
213 *TTLL5^{P371}*), which is required for anchoring TTL to α-tubulin by forming hydrogen bonds with
214 C-terminal tail residues of α-tubulin (Prota et al., 2013). However, the importance of
215 *TTLL5^{P371}* has not been reported in mammalian systems. Surprisingly, in *Drosophila*, P522
216 was also essential for glutamylation, revealing P522 as a novel critical residue for the
217 glutamylation function of TTLL5.

218

219

220 **Other PTMs of the C-terminal tail of ovarian α-tubulin**

221 Our MS results also detected glycylated C-terminal α-tubulin peptides in ovarian samples.
222 The glycylations were observed on the C-terminal tail of the *Drosophila* ovarian TBA1/3
223 isoforms but not on TBA4 **(Fig. S3A, S3B)**. Up to 2 glycines were primarily detected on
224 Glu443, Glu445, Glu448, or Glu449 of TBA1/3. The frequency of C-terminal peptides
225 containing Gly (G) modifications was similar or somewhat higher in *TTLL5* mutants
226 compared to the wild-type control **(Fig. S3C)**, suggesting that *TTLL5* is not needed for this
227 modification or even counteracts it.

228 Western blotting showed no or only minor changes in tyrosinated α-tubulin levels in any of
229 the null or CRISPR/Cas9 generated point mutants, and *TTLL5* overexpression also did not
230 affect these levels **(Fig. 3B, 3C, 3E).** TTLL5 levels, therefore, do not appear to affect levels
231 of tyrosinated α-tubulin in ovaries.

232

233 **Effect of *TTLL5* on Kinesin-1 dependent refinement of posterior localization of Staufen**

234 *osk* mRNA localization, combined with translation control, is essential for targeting Osk
235 protein expression to its proper posterior compartment in the cell (Suter, 2018; Weil, 2014).
236 Staufen is a ribonucleoprotein (RNP) that associates with *osk* mRNA during *osk* mRNA
237 localization. Staufen/*osk* mRNA localization requires the dynein/dynactin mediated minus-
238 end transport machinery in the early stages of oogenesis. Subsequently, the Staufen/*osk*
239 mRNA becomes localized to the posterior of the oocyte from mid to late stages of oogenesis.
240 This particular Staufen/*osk* mRNA localization phase within the oocyte depends on a
241 kinesin-driven process, including Kinesin-1 based active transport and ooplasmic streaming
242 in stage 10B (S10B) oocytes (Kato and Nakamura, 2012) (Lu et al., 2018) (Brendza et al.,
243 2000) (Zimyanin et al., 2008). To determine whether *TTLL5* contributes to this process, we
244 studied the role of *TTLL5* in dynein and kinesin transport by analyzing the localization of
245 Staufen in ovaries lacking functional TTLL5.

246 An established method to quantify the localization of Staufen to the posterior cortex is to
247 measure the length of the posterior Staufen crescent along the cortex (Lu et al., 2016). A
248 shorter crescent is a sign of better, tighter localization. We found that the length of the
249 posterior Staufen crescent was significantly increased in *TTLL5* null and *TTLL5* point mutant
250 ovaries compared to control ovaries (**Fig. 4A', 4A''', 4B-B')**. Furthermore, Z-stack images
251 revealed a more diffusely spread Staufen signal in all *TTLL5* mutants, although this varied
252 more between different samples **(Fig. 4A', 4B)**. The increased length of the crescent was

253 fully reversed to the regular length in all UAS-*Venus::TTLL5* rescued strains **(Fig. 4A''-A''')**.
254 We also analyzed the distribution of Venus::TTLL5 during oogenesis. Antibody staining
255 suggested that Venus::TTLL5 strongly accumulated in the oocyte, especially along the
256 cortex **(Fig. 4A'')**. In conclusion, the posterior localization refinement of Staufen in S10B
257 oocytes requires *TTLL5*. Because the point mutation blocks explicitly the enzymatic activity
258 of TTLL5, it appears that the proper localization requires glutamylation of tubulin.

259 To test if *TTLL5* is also required by the dynein/dynactin machinery and the Staufen/*osk*
260 mRNA transport during previtellogenic stages of oogenesis, we also imaged the localization
261 of Staufen and Bicaudal-D (BicD) proteins and *BicD* mRNA in early stages. BicD is the linker
262 that couples diverse cargos to the dynein/dynactin motor and is thus an excellent marker to
263 evaluate dynein transport function (Claussen and Suter, 2005). BicD and Staufen proteins,
264 and *BicD* and *osk* mRNAs showed similar localization patterns during early oogenesis when
265 comparing *TTLL5* mutants and control ovaries **(Fig. 4C)**. The expression of BicD was not
266 affected by the levels of TTLL5 as assessed by Western blotting (**Fig. 4D**, **Fig. S4**). These
267 results indicated that in ovaries, kinesin-dependent Staufen/*osk* localization processes
268 require *TTLL5*. In contrast, the dynein-dependent nurse cell to oocyte transport of mRNAs
269 and RNPs during early oogenesis does not appear to depend on *TTLL5*.

270

271 **Kinesin-1-dependent ooplasmic streaming in stage 10B oocytes requires *TTLL5***

272 Ooplasmic streaming is a bulk movement of the oocyte cytoplasm that circulates and
273 distributes mRNAs and proteins in the oocyte, including the Staufen/*osk* mRNA RNPs. It
274 allows these mRNA and proteins to reach their intended position, where they become
275 anchored. Slow and nondirectional flows initiate at stages 8–9 and are followed by rapid and
276 circular streaming at S10B (Lu et al., 2016). Kinesin-1-dependent microtubule sliding is
277 critical for this fast ooplasmic streaming (Lu et al., 2016). The kinesin-dependent final
278 posterior localization of Staufen in S10B oocytes depends on this process and *TTLL5*. Aside
279 from this, the TTLL5 protein was present in the cortical region of the oocyte **(Fig. 4A")**, the
280 region where the microtubule sliding occurs (Lu et al., 2018). We thus wanted to determine if
281 *TTLL5* contributes to an efficient kinesin-dependent sliding that drives ooplasmic streaming.

282 We firstly examined the levels of Kinesin-1 and found that they were neither affected in
283 *TTLL5* mutant ovaries nor in ovaries overexpressing *Venus::TTLL5* (**Fig. 5A, Fig. S4**). To
284 test if *TTLL5* is needed for ooplasmic streaming, we followed this process in real-time by
285 measuring vesicle movement in DIC time-lapse movies (**Mov. S1-S4**). We then tracked the

286 movement of the vesicles along the cortex region where microtubule sliding occurs (**Fig.**
287 **5B**). The velocity of the tracked vesicles was not affected in *TTLL5* mutant ovaries (**Fig. 5C**).
288 However, the analysis of the kymographs of these tracked vesicles showed that while control
289 ovaries have a typical streaming pattern with vesicles moving with a flow direction parallel to
290 the cortex, *TTLL5*^{MiEx} and *TTLL5*^{E517A} mutant ovaries displayed a disordered streaming
291 pattern (**Fig. 5D**). The typical streaming pattern was restored in *TTLL5*^{MiEx} ovaries
292 expressing a *Venus::TTLL5* rescue construct. Because the point mutation explicitly blocks
293 the enzymatic activity of TTLL5, our results suggest that TTLL5 is vital to control the
294 directionality of the fast ooplasmic streaming through its role in MT glutamylation.

295

296 **The transport of mitochondria in neurons depends on the glutamylation activity of**
297 **TTLL5**

298 Previous studies in *Drosophila* reported that *TTLL5* is required for the initiation of α-tubulin
299 glutamylation in the nervous system (Devambez et al., 2017). However, the absence of α-
300 tubulin glutamylation seemed not to be detrimental to the tested nervous system functions in
301 *Drosophila* (Devambez et al., 2017). The wing nerves are an attractive system to monitor
302 organelle transport such as the movement of mitochondria (Vagnoni and Bullock, 2016)
303 (Hollenbeck and Saxton, 2005). We thus used wing nerves to study neuronal transport in the
304 peripheral nervous system. Consistent with a previous report, we found that in extracts from
305 a mixture of heads and wings, α-tubulin was glutamylated, and this PTM depended on the
306 enzymatic activity of TTLL5 (**Fig. 6A)**; (Devambez et al., 2017). This suggests that the wing
307 nerve could be a suitable system for this test.

308 To study if neuronal transport of mitochondria in wing neurons depends on glutamylation of
309 α-tubulin, we tracked the movement of GFP-labelled mitochondria (Mito::GFP) in selected
310 areas of both the L1 and L3 wing veins of freshly eclosed flies (**Fig. 6B**). Time-lapse videos
311 of Mito::GFP movement in the L1 and L3 veins, respectively, are shown in **Mov. S5** and
312 **Mov. S6**, respectively. Motile mitochondria were manually tracked using the Fiji MTrackJ
313 plugin (**Fig. 6C**). Movies and still images clearly showed a decrease of motile mitochondria
314 in the region close to the arch of the L1 vein and no transported mitochondria in the L3 vein
315 of the *TTLL5*^{E517A} mutant, pointing to the importance of the enzymatic activity of TTLL5 for
316 proper transport. For quantitative analysis, the ratio of motile particles was calculated based
317 on the values divided by total particles from three wings of each genotype (**Fig. 6D**). The
318 total particles include all the static and transporting ones, which were counted based on the
319 signal from one chosen still image. Quantifications showed, firstly, that the total number of

320 particles in the L1 vein (384) was twice as high as in the L3 vein (186). This is likely because
321 the L1 vein contains more neurons than the L3 (Vagnoni and Bullock, 2016). Secondly,
322 however, in wild-type wings, the fraction of motile mitochondria is higher (24%) in L3 veins
323 than in L1 veins (7.8%). This might be because compared to the L3 vein, which consists
324 mainly of axons (Vagnoni and Bullock, 2016) (**Fig. S5**), the region closed to the arch of the
325 L1 vein contains not only axons but also several cell bodies and dendrites (Vagnoni and
326 Bullock, 2016) (**Fig. S5**). Mitochondria in dendrites are longer than in axons (Chang et al.,
327 2006). Longer mitochondria are less motile than short ones (Misgeld et al., 2007). Many less
328 motile mitochondria in cell bodies and dendrites "diluted" the motile mitochondria ratio
329 measured in L1 veins. Because axons are easily distinguishable in the L3 vein, the region of
330 L3 seemed to be a better choice for axonal transport studies than the one in the L1 vein. The
331 quantification of the motile ratio in the *TTLL5*^{E517A} mutant showed no motile mitochondria in
332 the L3 vein of the *TTLL5*^{E517A} mutant (**Fig. 6D**), strongly indicating that *TTLL5* is required for
333 the initiation of axonal transport of mitochondria. Apart from this, the quantification of the
334 motile ratio in the L1 showed a drop from 7.8% (plus-end 5.3% and minus-end 2.5%) in the
335 control to 1.9% in *TTLL5* ^{E517A} mutant wings (plus-end 1.5% and minus-end 0.4%) (**Fig. 6D**
336 and **Table 4**). These results reveal the importance of the enzymatic activity of *TTLL5* for *in*
337 *vivo* mitochondrial transport in wing nerves.

338 Because no motile mitochondria were found in the L3 region, we evaluated other
339 transport parameters in the L1 region. The *Drosophila* sensory neurons contain axons with
340 plus-end-out MTs and dendrites with minus-end-out MTs (Stone et al., 2008; Zheng et al.,
341 2008). Though the L1 region is enriched in a mix of axons, dendrites, and cell bodies, the
342 direction of the organelle transport can still be established. The mitochondria transported
343 towards the thorax of a fly move by plus-end transport, driven by kinesin, whereas
344 mitochondria transported away from the thorax are transported by dynein. We examined the
345 parameters of running patterns, trafficking length, and velocity of mitochondrial movement in
346 region L1. The start of a run was chosen at the time point when a motile particle began to
347 move from a stationary position, and the stop of a run was defined when the particle stopped
348 moving. The pausing of a run is indicated by the particle moving at a rate lower than 0.2
349 μm/s. Particles with speeds higher than 0.2 μm/s were considered "trafficking". A schematic
350 running pattern is shown in **Fig. 6E.** Bidirectionally moving particles were seen only very
351 rarely in our case. In these cases, they usually moved a short distance towards one
352 direction, suddenly turned back, and ran in the opposite direction. For the plus-end transport
353 (**Table 4)**, the average total duration of a running time showed no significant difference
354 between controls (92s) and *TTLL5* mutants (98s). As well, no significant difference in the
355 mean velocity of the tracked mitochondria was observed between controls (0.37 μm/s) and

356 *TTLL5*^{E517A} mutants (0.36 μm/s). However, the average pausing time ratio in *TTLL5*^{E517A}
357 (63%) showed a decrease compared to the control (74%), suggesting that α-tubulin
358 glutamylation was required for attaching and holding or stopping mitochondria during their
359 whole "run" along MTs (see **Fig. 6E**). Consistent with this observation, mitochondria in
360 *TTLL5*^{E517A} moved longer distances (12μm) per run than the mitochondria observed in the
361 controls (7μm). Even though our research focused on the plus-end transport, preliminary
362 numbers for the minus-end transport suggest that the motile frequency, total duration, and
363 pausing time ratio might decrease in *TTLL5*^{E517A} (**Table 4**). However, the small numbers for
364 *TTLL5*^{E517A} do not allow this conclusion.

365 It appears that two different mechanisms are involved between the start and the ongoing
366 transport of individual mitochondria. In the first step, the lack of glutamylation hinders the
367 initiation of the axonal transport of mitochondria, indicating that the *in vivo* initiation of
368 processive axonal transport heavily depends on glutamylation. Once mitochondria have
369 started to move, the lack of α-tubulin glutamylation increases the plus-end trafficking time
370 and trafficking length of the mitochondria in a region of the wing nerve that contains axons,
371 dendrites, and cell bodies, indicating that glutamylation is also needed for holding or
372 anchoring mitochondria on the MTs during trafficking in neurons. Altogether, these results
373 demonstrate the role of α-tubulin glutamylation in the efficient mitochondrial transport in wing
374 nerves.

375

Discussion

Both Western blotting and MS results from wild-type and mutant *Drosophila* revealed that *TTLL5* is essential for mono- and polyglutamylation of α-tubulin in ovaries. The complete lack of even monoglutamylated tubulin tails in the presumptive null mutants of *TTLL5* strongly suggests a requirement for TTLL5 for adding the first branching Glu to the Glu side chains in the C-term. The requirement for adding the first Glu could also account for the lack of polyglutamylation in the mutants. This result is consistent with results from HeLa cells and the *Drosophil*a nervous system (Devambez et al., 2017; van Dijk et al., 2007). Further MS results indicated that *TTLL5* specifically functions to glutamylate the TBA1/3 but not the TBA4 isoforms of α-tubulin. Up to three Glu residues were found added to the positions E443/E445/E448/E449 of TBA1/3 (**Fig. 1A, 1B**). Even though TBA4 is an ovarian-specific isoform, our MS analysis showed a lower amount of TBA4 peptides than TBA1/3 peptides (**Table S3**), suggesting that it accumulated at a lower level in ovaries. It thus seems that the qualitative difference this isoform provides is more important for oogenesis than simply providing additional α-tubulins. Aside from the differences in the primary sequence, this isoform appears to be glutamylation resistant. The evolutionary appearance of a non-glutamylatable α-tubulin isoform may indicate that this tissue needs special microtubules that regulate the rate of different transport processes by altering the rate of glutamylated/non-glutamylated MTs.

Our MS analysis revealed that polyglycylation of α-tubulin also occurs in the ovarian tissue and that glycylation modifies the same sites in the C-terminal domain as polyglutamylation does, the side chains of the Glutamic acid residues. Because glycylation is still seen in the *TTLL5* mutants, TTLL5 does not seem to be the enzyme for this reaction and glutamylation of one site is not a prerequisite for glycylation of another site. It would now be interesting to find out whether glycylation even serves to prevent glutamylation or competes with it and whether this is used as another level of control of microtubule activity. In *Tetrahymena*, such a competition has been described because there, Glutamic acid and Glycine ligases compete for the same sites or affect each other by sterically blocking adjacent sites of tubulins (Redeker et al., 2005; Wloga et al., 2009). Only a surprisingly small fraction of the *TTLL* family is expressed in *Drosophila* ovaries, according to Flybase. Aside from *TTLL5*, we only found evidence for the expression of *TTLL4A* and *TTLL12* **(Table S2)**. Our genetic analysis of *TTLL5* showed that it is not required for glycylation.

The predicted mouse homolog of the *Drosophila TTLL4A* was found to glutamylate β-tubulin (Mahalingan et al., 2020), suggesting that this isoform could be required for β-tubulin

410 glutamylation in ovaries. The function of the predicted homolog of *Drosophila TTLL12* in
411 mammals was poorly studied, and the core TTL domain of mouse TTLL12 is less conserved
412 than other mouse E- and G- ligases of the TTLL family (van Dijk et al., 2007). It is, therefore,
413 unclear yet which enzyme performs the polyglycylation of α-tubulin in *Drosophila* ovaries.

414 The ooplasmic streaming process is required for the posterior localization of Staufen/*osk*
415 mRNA and is mediated by an MT-sliding mechanism (Lu et al., 2016). This MT-sliding, an
416 essential step for normal oogenesis, involves sliding between the cortically anchored
417 microtubules and the free cytoplasmic microtubules close to the cortex. This sliding between
418 the two classes of microtubules is Kinesin-1 dependent. Our data show that *TTLL5* is
419 needed for normal oocyte cytoplasmic streaming and the posterior localization of
420 Staufen/*osk mRNA*, suggesting that it affects these processes through a role in kinesin-1-
421 dependent MT sliding.

422 It is worth pointing out that *in vitro* studies demonstrated that the artificial tethering of
423 glutamyl peptides to the side chains of both α- and β-tubulin increased the run length of
424 Kinesin-1 on tubulins (Sirajuddin et al., 2014). *Drosophila TTLL5* is essential for
425 glutamylation of α-tubulin but not for β-tubulin. These results provide the best evidence yet
426 that *TTLL5*-mediated glutamylation of α-tubulin plays a vital role in Kinesin-1-driven
427 processes *in vivo*. However, the phenotypes, including ooplasmic streaming and Staufen
428 localization, observed in *TTLL5* mutants were not as severe as the ones that arose when
429 (Kinesin heavy chain) KHC was not functional (Lu et al., 2016). Besides, in the wing nerve
430 experiment, though the initiation of mitochondrial transport was heavily dependent on the
431 glutamylation of α-tubulin, some "leaky" ones still started to be transported in *TTLL5*
432 mutants. This seems to suggest that some Kinesin-1-dependent processes can still operate
433 as long as glutamylation of β-tubulin is present.

434 In *KHC* mutants, there is an overall decrease in kinesin-dependent anterograde and the
435 dynein-driven retrograde transport of mitochondria in *Drosophila* larval motor axons (Pilling
436 et al., 2006). We observed a similar loss of motile mitochondria in the axon-rich region in the
437 *TTLL5*^{E517A} mutant wing (**Fig. 6C, 6D**). Because both previous studies (Devambez et al.,
438 2017) and our data (**Fig. 6A**) showed that *TTLL5* was required for α-tubulin glutamylation in
439 the nervous system, all these results suggested that α-tubulin glutamylation is a crucial
440 factor for the Kinesin-1 mediated initiation of mitochondrial transport in axons.

441 By analyzing the dynamics of the few motile mitochondria observed in mutant L1 veins,
442 we found that in the absence of glutamylation, the plus-end mitochondria can run longer
443 distances with shorter pausing times (**Fig. 6G**). Interestingly, a recent study linked the

444 reduced trafficking time of mitochondria during axonal transport to neurodegeneration in
445 mice, which was caused by hyperglutamylation of α-tubulin but not β-tubulin (Bodakuntla et
446 al., 2021). It thus strongly indicated that the glutamylation of α-tubulin causes the halting of
447 the ongoing transport of single mitochondria *in vivo*. Because of the orientation of the MTs in
448 the *Drosophila* wing neurons is unidirectional and the plus-end transport of mitochondria was
449 affected in the absence of the glutamylation of α-tubulin, we now learned that glutamylation
450 is at least needed for the Kinesin-1-based transport.

451 Aside from traffic jams, several mechanisms have been found to stop mitochondrial
452 transport in neurons. For instance, tethering mitochondria to the actin cytoskeleton (Pathak
453 et al., 2010), blocking the binding of Kinesin-1 to MTs by increasing Ca^{2+} (Wang and
454 Schwarz, 2009), or abolishing the interaction between Kinesin-1 and mitochondria by
455 degrading one of the linker proteins, Miro (Wang et al., 2011). Here, we provided *in vivo*
456 evidence that glutamylation of MTs is an essential regulatory mechanism that contributes to
457 the sophisticated neuronal mitochondrial transport system.

458

459 **Materials and methods**

460

461 ***Drosophila* genetics**

462 The fly stocks used in this study, MattubGal4 (7062), *TTLL5*^{pBac} (16140), *TTLL5*^{Mi} (32800),
463 and *Df(3R)BSC679* (26531), were obtained from the Bloomington Drosophila stock center.
464 The *TTLL5*^{MiEx} mutation was made by imprecise excision of the Minos element, which left a 3
465 base insertion (CTA) that introduces a premature stop codon at genomic position 8,132 in
466 the open reading frame (polypeptide position 392). The different *TTLL5* point mutations were
467 generated by CRISPR/Cas9. The two *Drosophila* stocks used for *TTLL5* gene editing, *y[1]*
468 *M{w[+mC]=nos-Cas9.P}ZH-2A w[*]* and *y[1] v[1] P{y[+t7.7]=nos-phiC31\int.NLS};*
469 *P{y[+t7.7]=CaryP} attP40* were obtained from the Bloomington *Drosophila* Stock Center
470 (54591) (Port et al., 2014) and (25709), respectively. Target sequences near the K131, R339
471 R376, and E517 codons were selected to introduce INDELs and the following point
472 mutations: K131A, R339A (b6-7 loop), R376A, and E517A. Phosphorylated and annealed
473 primers (Table S1A) needed to construct the corresponding coding sequences for a single
474 guide RNA (sgRNA) were each cloned into the BbsI site of *pCFD5* according to the protocol
475 published on www.crisprflydesign.org. After amplifying the vector in XL1 blue cells, the
476 plasmids were sequenced to verify correct assembly. Subsequently, they were injected into
477 *attP40* embryos. TTLL5-guide stocks with integrated genes encoding sgRNAs were
478 established *(=v; attP40{v*$^{+}$*, TTLL5-guide}/CyO*). To obtain INDELs for TTLL5, a three-
479 generation crossing schema was set up. Firstly, *nos-cas9* virgins were crossed with males
480 from the different TTLL5-guide stocks. Secondly, the subsequent single male progeny was
481 crossed with *w; Ly/TM3, Sb* virgins. Thirdly, the resulting single *TM3, Sb* males were again
482 crossed with *w; Ly/TM3, Sb* virgins to establish the stocks. The nature of the mutated *TTLL5*
483 gene in each stock was determined by sequencing. To introduce specific point mutations in
484 the *TTLL5* gene, embryos from a cross with *y w {w*$^{+}$*, nos-cas9}* virgins and TTLL5-guide
485 males were injected with the appropriate template (**Table S1B).** The resulting individual adult
486 males were crossed with *w; Ly / TM3, Sb* virgins, and stocks were established. The
487 presence of a mutated *TTLL5* gene was confirmed by restriction digestion and subsequent
488 sequencing. All *TTLL5* alleles were crossed to *Df(3R)BSC679* to test the effect of the *TTLL5*
489 mutations in hemizygous animals. The *UASp-venus::TTLL5* DNA construct was made from
490 the *TTLL5* cDNA amplified by PCR (forward primer: 5′ -
491 GTTCAGATCTATGCCTTCTTCATTGTGTG -3′; reverse primer: 5′ -
492 GAGTCATTCTAGAGCTTCATAGAAATACCTTCTCC- 3′) and inserted into the *pUASP-*
493 *venus* vector via Xba I/Bgl II ligation. DNA was inserted into the *attP-58A* landing platform

494 (24484) to generate the transgenetic *UASp-venus::TTLL5* fly strain. *ApplGal4* and *UAS-*
495 *mito::GFP* were kindly provided by Simon Bullock's group (Vagnoni et al., 2016).

496

497 **Western blotting**

498 Western blotting performed with ovarian extracts was carried out with 10-20 pairs of ovaries
499 for each genotype. Newly hatched females of the indicated genotypes were collected and
500 crossed with *w* males in fresh vials with ample yeast food for two days. Fully developed
501 ovaries were then dissected and collected. To analyze neuronal samples, a mixture of head
502 and wing tissue from 30 flies was collected for each genotype. The samples were directly
503 lysed in Laemmli buffer, boiled at 95°C for 10 min, and analyzed by SDS-PAGE.
504 Chemiluminescence detection was done with the Amersham imager 600 (GE healthcare).
505 The following primary antibodies were used: mouse 1D5 (1:500, Synaptic System), mouse
506 GT335 (1:200, Adipogen), mouse DM1A (1:1,000, Sigma), mouse tyrosinated α-tubulin
507 (1:1,000, Sigma), rabbit GFP (1:2,000, Sigma), rabbit GAPDH (1:1,000, GeneTex), rabbit
508 TTLL5 (1:500, GenScript), mouse BicD (1B11 plus 4C2, 1:5) (Suter and Steward, 1991),
509 rabbit KHC (1:1,000, cytoskeleton), rabbit β-monoE (1:1,000) (Bodakuntla et al., 2021).
510 Secondary antibodies were HRP-linked goat anti-mouse (1:1,0000, GE Healthcare) and
511 HRP-linked goat anti-rabbit (1:10,000, GE Healthcare). Antibodies were incubated in 5%
512 non-fat milk PBST (PBS with 0.1 % Triton X-100) and washed with PBST.

513

514 **Immunoprecipitations (IPs) and Mass Spectrometry**

515 Proteins were extracted from the ovaries of 100 3-day-old, well-fed females of each
516 genotype, crossed to wild-type males, and proteins were immunoprecipitated with an α-
517 tubulin antibody (Sigma) bound to G-protein coupled magnetic beads. Samples (ligated with
518 beads) were boiled and run on SDS-PAGE. These were then stained with Coomassie Blue.
519 The gel pieces containing the α-tubulin region were cut, alkylated, and digested by trypsin N
520 (ProtiFi) for 3 hours at 55°C. C-terminal peptides of α-tubulin were analyzed by liquid
521 chromatography (LC)-MS/MS (PROXEON coupled to a QExactive mass spectrometer,
522 Thermo Fisher Scientific). Samples were searched against the UniProtKB *Drosophila*
523 database using Pipeline, PEAKS, Easyprot and MSfragger as search engines. Peptides
524 were shown by PSM value (peptide spectrum match). To avoid repetition of total PSM
525 quantification, we searched only for one type of PTM in an analysis per time. Total PSM

526 indicates the sum of PSMs of primary C-terminal peptides with either glutamylation or
527 glycylation modifications, or non-modified peptides.

528

529 **Ooplasmic streaming in live oocytes**

530 Three days old females were kept together with wild-type males under non-crowding
531 conditions at 25°C on food containing dry yeast. The determination of ooplasmic streaming
532 was based on the method of Lu and colleagues (Lu et al., 2016). Ovaries were directly
533 dissected in 10S halocarbon oil (VWR) and eggs were teased apart in the oil drop on a
534 24×50 mm coverslips (VWR). Living stage 10B oocytes were directly observed and imaged
535 with the 60×1.4 NA oil immersion objective on a Nikon W1 LIPSI spinning disk with a
536 2x Photometrics Prime BSI CMOS camera. Time-lapse images were acquired every 2s for 2
537 min under bright-field (BF) controlled by Nikon Elements software. Flow tracks were
538 generated by kymographs using the Fiji (Schindelin et al., 2012) plugin Multi Kymograph
539 (HTTPS:// imagej.net/ Multi _Kymograph). The velocity of 100-200 particles/ooplasm was
540 tracked using Analysis > Distribution of Speed (Track-Based) by DiaTrack 3.05 (Vallotton
541 and Olivier, 2013), with a maximum jumping distance of 3.24 μm/s. The datasets were
542 exported to Excel, where the mean velocities of each ooplasm were analyzed. Then the
543 velocities of different ooplasms from different genotypes were shown as means ± SEM by
544 Prism 5 software (GraphPad).

545

546 ***In situ* hybridization, Immunostaining, and confocal microscopy**

547 Plasmids containing *BicD* and *osk* cDNA were used as templates to generate digoxigenin- or
548 Fluorescein (FITC)-labeled RNA antisense probes. *In situ* hybridization experiments on
549 ovaries were performed as described (Vazquez-Pianzola et al., 2011). Ovaries were
550 dissected in 1× PBS and fixed in buffer (200 μl 4% formaldehyde (Sigma), 600 μl Heptane
551 (Merck Millipore), 20 μl DMSO (Sigma) for each group) for 20 min. Then ovaries were
552 blocked in 5% milk powder in PBT (PBS, 0.1% Tween). The digoxigenin-labeled probes
553 were detected with sheep-anti-digoxigenin antibodies (1:1,000, Jackson ImmunoResearch)
554 and donkey anti-sheep 647 (1:200, Jackson ImmunoResearch). Fluorescein-labeled probes
555 were detected with mouse anti-fluorescein antibodies (1:1,000, Roche) and donkey anti-
556 mouse 488 antibodies (1:1,000, Jackson Immunoresearch). For Staufen and BicD protein
557 staining, ovaries were incubated with rabbit anti-Staufen (1:2,000) (St Johnston et al., 1991),

558 mouse anti-BicD (1B11 plus 4C2, 1:5) (Suter and Steward, 1991) and rabbit anti-GFP
559 (1:200, Sigma) antibodies at 4°C overnight, and incubated with secondary Alexa Fluor goat
560 anti-mouse 647 (1:400, Jackson ImmonoResearch) and Alexa Fluor goat anti-rabbit 488
561 (1:400, Life technologies Thermo Fischer) at room temperature for 3h. DNA and nuclei were
562 stained using Hoechst 33528 (Thermo Fischer Scientific) for 10 min. Mounted samples were
563 imaged with a Leica TCS SP8 confocal microscope equipped with a 63×1.40 oil lens and
564 controlled by the Las X software (Leica). Images of single focal planes and 12 μm Z
565 projection were acquired. The crescent length of Staufen was processed by the Fuji
566 segmented line tool based on the single plane. The data were shown as means ± SEM by
567 Prism 5 (GraphPad software). The statistical significance was determined by an unpaired
568 two-tailed non-parametric t-test (Mann-Whitney test).

569

570 **Mitochondrial transport in *Drosophila* wing neurons**

571 Mitochondrial transport in *Drosophila* wing neurons was tracked as described (Vagnoni and
572 Bullock, 2016). In brief, newly eclosed flies were anesthetized with CO_2 and immobilized in a
573 custom-built chamber formed of two No.1.5 24×50 mm coverslips (VWR). Imaging of wings
574 was performed with a Nikon W1 LIPSI spinning disk microscope equipped with a 2x
575 Photometrics Prime BSI CMOS camera and a 60×1.4 NA oil immersion lens. Time-lapse
576 video of a single focal plane was acquired with an acquisition rate of 0.5 frame/s for 3 min for
577 Mito::GFP using a 488 nm laser.

578 Quantification of the movements was performed in Fiji. A region close to the axonal tract of
579 the wing arch of the L1 vein and a region of the L3 vein were selected and straightened with
580 the Straighten plugin (Eva Kocsis, NIH, MD). For each “run”, the total run distance of more
581 than 2 μm was defined as “transported or motile mitochondria”. To exclude the oscillatory
582 movements of mitochondria, a minimal instant velocity between each frame was defined at
583 0.2 μm/s. Transported mitochondria were manually marked with MTrackJ plugin (Meijering
584 et al., 2012) and tracked by the manual tracking plugin (Fabrice Cordelières, Institute Curie,
585 France). The total number of mitochondria was counted from a single frame using Fiji's
586 “Analyze particle” function. Run-length, velocity values, and total running & pausing times
587 were exported into Excel for analysis. The data were shown as means ± SEM by Prism 5
588 (GraphPad). The statistical significance was determined with the student’s t-test.

589

590 **Sequence alignment**

591 Sequences were aligned by CLC Sequence Viewer 8.0 software (Qiagen). The UniProtKB
592 accession numbers are as follows: *HsTTL*: Q8NG68; *HsTTLL5*: Q6EMB2; *MmTTLL5*:
593 Q8CHB8; *DmTTLL5*: Q9VBX5.

594

595 **Acknowledgments**

596 We thank Carsten Janke (Institute Curie, France) for anti-β-monoE antibodies, Simon L.
597 Bullock (Cambridge, UK) for *ApplGal4* and *UAS-mito::GFP* fly lines, Michel Steinmetz (Paul
598 Scherrer Institute, Switzerland), and the Janke laboratory members for discussions, and
599 suggestions. We also thank the Mass Spectrometry center (University of Bern, Switzerland)
600 members Sophie Braga Lagache and Natasha Buchs for performing the MS experiments
601 and Manfred Heller and Anne-Christine Uldry for peptide analysis and discussion of the
602 results.

603

604 **Support**

605 This work was financially supported by the project grants 31003A_173188 and
606 310030_205075 from the Swiss National Science Foundation (SNF; https://www.snf.ch/en)
607 to BS. Equipment support was by an equipment grant from SNF (316030_150824) to BS
608 and by the University of Bern (https://www.unibe.ch). Additional salary and material support
609 were received from the University of Bern (https://www.unibe.ch) to BS. The funders had no
610 role in the study design, data collection and analysis, decision to publish, or manuscript
611 preparation.

612 The authors declare no competing financial interests.

613 Author contributions: Mengjing Bao, Beat Suter, and Maria Paula Vazquez-Pianzola
614 conceived the project and designed the experiments. Mengjing Bao, Beat Suter, Ruth Dörig,
615 and Dirk Beuchle performed the experiments and analyzed the data; Mengjing Bao and Beat
616 Suter wrote the manuscript.

617

618

619 **References**

620 Arce, C.A., J.A. Rodriguez, H.S. Barra, and R. Caputo. 1975. Incorporation of L-tyrosine, L-
621 phenylalanine and L-3,4-dihydroxyphenylalanine as single units into rat brain tubulin.
622 *Eur J Biochem*. 59:145-149.

623 Bodakuntla, S., X. Yuan, M. Genova, S. Gadadhar, S. Leboucher, M.C. Birling, D. Klein, R.
624 Martini, C. Janke, and M.M. Magiera. 2021. Distinct roles of α- and β-tubulin
625 polyglutamylation in controlling axonal transport and in neurodegeneration. *EMBO J*.
626 40:e108498.

627 Brendza, R.P., L.R. Serbus, J.B. Duffy, and W.M. Saxton. 2000. A function for kinesin I in
628 the posterior transport of oskar mRNA and Staufen protein. *Science*. 289:2120-2122.

629 Chang, D.T., A.S. Honick, and I.J. Reynolds. 2006. Mitochondrial trafficking to synapses in
630 cultured primary cortical neurons. *J Neurosci*. 26:7035-7045.

631 Claussen, M., and B. Suter. 2005. BicD-dependent localization processes: from Drosophilia
632 development to human cell biology. *Ann Anat*. 187:539-553.

633 Devambez, I., J. van Dijk, S. Benlefki, S. Layalle, Y. Grau, K. Rogowski, M.L. Parmentier,
634 and L. Soustelle. 2017. Identification of DmTTLL5 as a Major Tubulin Glutamylase in
635 the Drosophila Nervous System. *Sci Rep*. 7:16254.

636 Eddé, B., J. Rossier, J.P. Le Caer, E. Desbruyères, F. Gros, and P. Denoulet. 1990.
637 Posttranslational glutamylation of alpha-tubulin. *Science*. 247:83-85.

638 Gadadhar, S., G. Alvarez Viar, J.N. Hansen, A. Gong, A. Kostarev, C. Ialy-Radio, S.
639 Leboucher, M. Whitfield, A. Ziyyat, A. Touré, L. Alvarez, G. Pigino, and C. Janke.
640 2021. Tubulin glycylation controls axonemal dynein activity, flagellar beat, and male
641 fertility. *Science*. 371.

642 Gadadhar, S., S. Bodakuntla, K. Natarajan, and C. Janke. 2017. The tubulin code at a
643 glance. *J Cell Sci*. 130:1347-1353.

644 Hallak, M.E., J.A. Rodriguez, H.S. Barra, and R. Caputto. 1977. Release of tyrosine from
645 tyrosinated tubulin. Some common factors that affect this process and the assembly
646 of tubulin. *FEBS Lett*. 73:147-150.

647 Hollenbeck, P.J., and W.M. Saxton. 2005. The axonal transport of mitochondria. *J Cell Sci*.
648 118:5411-5419.

649 Janke, C., K. Rogowski, D. Wloga, C. Regnard, A.V. Kajava, J.M. Strub, N. Temurak, J. van
650 Dijk, D. Boucher, A. van Dorsselaer, S. Suryavanshi, J. Gaertig, and B. Eddé. 2005.
651 Tubulin polyglutamylase enzymes are members of the TTL domain protein family.
652 *Science*. 308:1758-1762.

653 Kalfayan, L., and P.C. Wensink. 1982. Developmental regulation of Drosophila alpha-tubulin
654 genes. *Cell*. 29:91-98.

655 Kato, Y., and A. Nakamura. 2012. Roles of cytoplasmic RNP granules in intracellular RNA
656 localization and translational control in the Drosophila oocyte. *Dev Growth Differ*.
657 54:19-31.
658 L'Hernault, S.W., and J.L. Rosenbaum. 1985. Chlamydomonas alpha-tubulin is
659 posttranslationally modified by acetylation on the epsilon-amino group of a lysine.
660 *Biochemistry*. 24:473-478.
661 Lee, G.S., Y. He, E.J. Dougherty, M. Jimenez-Movilla, M. Avella, S. Grullon, D.S. Sharlin, C.
662 Guo, J.A. Blackford, Jr., S. Awasthi, Z. Zhang, S.P. Armstrong, E.C. London, W.
663 Chen, J. Dean, and S.S. Simons, Jr. 2013. Disruption of Ttll5/stamp gene (tubulin
664 tyrosine ligase-like protein 5/SRC-1 and TIF2-associated modulatory protein gene) in
665 male mice causes sperm malformation and infertility. *J Biol Chem*. 288:15167-15180.
666 Lu, W., M. Lakonishok, A.S. Serpinskaya, D. Kirchenbüechler, S.C. Ling, and V.I. Gelfand.
667 2018. Ooplasmic flow cooperates with transport and anchorage in. *J Cell Biol*.
668 217:3497-3511.
669 Lu, W., M. Winding, M. Lakonishok, J. Wildonger, and V.I. Gelfand. 2016. Microtubule-
670 microtubule sliding by kinesin-1 is essential for normal cytoplasmic streaming in
671 Drosophila oocytes. *Proc Natl Acad Sci U S A*. 113:E4995-5004.
672 Magiera, M.M., and C. Janke. 2014. Post-translational modifications of tubulin. *Curr Biol*.
673 24:R351-354.
674 Mahalingan, K.K., E. Keith Keenan, M. Strickland, Y. Li, Y. Liu, H.L. Ball, M.E. Tanner, N.
675 Tjandra, and A. Roll-Mecak. 2020. Structural basis for polyglutamate chain initiation
676 and elongation by TTLL family enzymes. *Nat Struct Mol Biol*. 27:802-813.
677 McKenney, R.J., W. Huynh, R.D. Vale, and M. Sirajuddin. 2016. Tyrosination of α-tubulin
678 controls the initiation of processive dynein-dynactin motility. *Embo j*. 35:1175-1185.
679 Meijering, E., O. Dzyubachyk, and I. Smal. 2012. Methods for cell and particle tracking.
680 *Methods Enzymol*. 504:183-200.
681 Misgeld, T., M. Kerschensteiner, F.M. Bareyre, R.W. Burgess, and J.W. Lichtman. 2007.
682 Imaging axonal transport of mitochondria in vivo. *Nat Methods*. 4:559-561.
683 Pathak, D., K.J. Sepp, and P.J. Hollenbeck. 2010. Evidence that myosin activity opposes
684 microtubule-based axonal transport of mitochondria. *J Neurosci*. 30:8984-8992.
685 Pilling, A.D., D. Horiuchi, C.M. Lively, and W.M. Saxton. 2006. Kinesin-1 and Dynein are the
686 primary motors for fast transport of mitochondria in Drosophila motor axons. *Mol Biol*
687 *Cell*. 17:2057-2068.
688 Port, F., H.M. Chen, T. Lee, and S.L. Bullock. 2014. Optimized CRISPR/Cas tools for
689 efficient germline and somatic genome engineering in Drosophila. *Proc Natl Acad Sci*
690 *U S A*. 111:E2967-2976.

691 Preston, S.F., G.G. Deanin, R.K. Hanson, and M.W. Gordon. 1979. The phylogenetic
692 distribution of tubulin:tyrosine ligase. *J Mol Evol*. 13:233-244.
693 Prota, A.E., M.M. Magiera, M. Kuijpers, K. Bargsten, D. Frey, M. Wieser, R. Jaussi, C.C.
694 Hoogenraad, R.A. Kammerer, C. Janke, and M.O. Steinmetz. 2013. Structural basis
695 of tubulin tyrosination by tubulin tyrosine ligase. *J Cell Biol*. 200:259-270.
696 Redeker, V., N. Levilliers, J.M. Schmitter, J.P. Le Caer, J. Rossier, A. Adoutte, and M.H. Bré.
697 1994. Polyglycylation of tubulin: a post-translational modification in axonemal
698 microtubules. *Science*. 266:1688-1691.
699 Redeker, V., N. Levilliers, E. Vinolo, J. Rossier, D. Jaillard, D. Burnette, J. Gaertig, and M.H.
700 Bré. 2005. Mutations of tubulin glycylation sites reveal cross-talk between the C
701 termini of alpha- and beta-tubulin and affect the ciliary matrix in Tetrahymena. *J Biol*
702 *Chem*. 280:596-606.
703 Redeker, V., R. Melki, D. Promé, J.P. Le Caer, and J. Rossier. 1992. Structure of tubulin C-
704 terminal domain obtained by subtilisin treatment. The major alpha and beta tubulin
705 isotypes from pig brain are glutamylated. *FEBS Lett*. 313:185-192.
706 Rüdiger, A.H., M. Rüdiger, J. Wehland, and K. Weber. 1999. Monoclonal antibody ID5:
707 epitope characterization and minimal requirements for the recognition of
708 polyglutamylated alpha- and beta-tubulin. *Eur J Cell Biol*. 78:15-20.
709 Schindelin, J., I. Arganda-Carreras, E. Frise, V. Kaynig, M. Longair, T. Pietzsch, S.
710 Preibisch, C. Rueden, S. Saalfeld, B. Schmid, J.Y. Tinevez, D.J. White, V.
711 Hartenstein, K. Eliceiri, P. Tomancak, and A. Cardona. 2012. Fiji: an open-source
712 platform for biological-image analysis. *Nat Methods*. 9:676-682.
713 Sirajuddin, M., L.M. Rice, and R.D. Vale. 2014. Regulation of microtubule motors by tubulin
714 isotypes and post-translational modifications. *Nat Cell Biol*. 16:335-344.
715 St Johnston, D., D. Beuchle, and C. Nüsslein-Volhard. 1991. Staufen, a gene required to
716 localize maternal RNAs in the Drosophila egg. *Cell*. 66:51-63.
717 Stone, M.C., F. Roegiers, and M.M. Rolls. 2008. Microtubules have opposite orientation in
718 axons and dendrites of Drosophila neurons. *Mol Biol Cell*. 19:4122-4129.
719 Suter, B. 2018. RNA localization and transport. *Biochim Biophys Acta Gene Regul Mech*.
720 1861:938-951.
721 Suter, B., and R. Steward. 1991. Requirement for phosphorylation and localization of the
722 Bicaudal-D protein in Drosophila oocyte differentiation. *Cell*. 67:917-926.
723 Theurkauf, W.E., H. Baum, J. Bo, and P.C. Wensink. 1986. Tissue-specific and constitutive
724 alpha-tubulin genes of Drosophila melanogaster code for structurally distinct proteins.
725 *Proc Natl Acad Sci U S A*. 83:8477-8481.
726 Vagnoni, A., and S.L. Bullock. 2016. A simple method for imaging axonal transport in aging
727 neurons using the adult Drosophila wing. *Nat Protoc*. 11:1711-1723.

728 Vallotton, P., and S. Olivier. 2013. Tri-track: free software for large-scale particle tracking.
729 *Microsc Microanal*. 19:451-460.
730 van Dijk, J., K. Rogowski, J. Miro, B. Lacroix, B. Eddé, and C. Janke. 2007. A targeted
731 multienzyme mechanism for selective microtubule polyglutamylation. *Mol Cell*.
732 26:437-448.
733 Vazquez-Pianzola P, Urlaub H, Suter B. Pabp binds to the osk 3'UTR and specifically
734 contributes to osk mRNA stability and oocyte accumulation. *Dev Biol*. 2011 Sep
735 15;357(2):404-18.
736 Wang, X., and T.L. Schwarz. 2009. The mechanism of Ca2+ -dependent regulation of
737 kinesin-mediated mitochondrial motility. *Cell*. 136:163-174.
738 Wang, X., D. Winter, G. Ashrafi, J. Schlehe, Y.L. Wong, D. Selkoe, S. Rice, J. Steen, M.J.
739 LaVoie, and T.L. Schwarz. 2011. PINK1 and Parkin target Miro for phosphorylation
740 and degradation to arrest mitochondrial motility. *Cell*. 147:893-906.
741 Weil, T.T. 2014. mRNA localization in the Drosophila germline. *RNA Biol*. 11:1010-1018.
742 Wloga, D., D.M. Webster, K. Rogowski, M.H. Bré, N. Levilliers, M. Jerka-Dziadosz, C. Janke,
743 S.T. Dougan, and J. Gaertig. 2009. TTLL3 Is a tubulin glycine ligase that regulates
744 the assembly of cilia. *Dev Cell*. 16:867-876.
745 Wolff, A., B. de Néchaud, D. Chillet, H. Mazarguil, E. Desbruyères, S. Audebert, B. Eddé, F.
746 Gros, and P. Denoulet. 1992. Distribution of glutamylated alpha and beta-tubulin in
747 mouse tissues using a specific monoclonal antibody, GT335. *Eur J Cell Biol*. 59:425-
748 432.
749 Zheng, Y., J. Wildonger, B. Ye, Y. Zhang, A. Kita, S.H. Younger, S. Zimmerman, L.Y. Jan,
750 and YN Jan. 2008. Dynein is required for polarized dendritic transport and uniform
751 microtubule orientation in axons. *Nat Cell Biol*. 10:1172-1180.
752 Zimyanin, V.L., K. Belaya, J. Pecreaux, M.J. Gilchrist, A. Clark, I. Davis, and D. St Johnston.
753 2008. In vivo imaging of oskar mRNA transport reveals the mechanism of posterior
754 localization. *Cell*. 134:843-853.

755

756 **Table 1) Role of *TTLL5* for the glutamylation of the C-terminal domain of TBA1/3.**

757 Frequency of glutamylated C-terminal peptides (containing the entire primary sequence) in *w* controls,
758 *TTLL5*^{pBac} and *TTLL5*^{MiEx} mutants containing modifications of 1E, 2E or 3Es.

	w (n=56)[1)]	*TTLL5*^{pBac} (n=29) (*%E mod*)	*TTLL5*^{MiEx} (n=7)
+1	41	0	0
+2	14	0	0
+3	7	0	0
Total Glu modifications[2)]	62	0	0

759 [1)] N indicates the values of total PSM (peptide spectrum match) of the full primary C-terminal TBA1/3 sequence.
760 [2)] Total Glu modification shows the sum of the three frequencies. The ratio was quantified based on the
761 glutamylated C-terminal TBA1/3 PSM values divided by total PSM.

762

763

764 **Table 2) Conservation between mammalian *TTLL5 and Drosophila TTLL5***

765 Residues labeled in red are critical residues for α-tubulin glutamylation by murine TTLL5 and are
766 conserved in human and *Drosophila* TTLL5 (van Dijk et al., 2007).

	K131 β6-7 loop (R188) R225 E366 N368
Mm TTLL5	TRKDR—KPVASSRGRG[1)]VY---VRLYVL---LLEVNLSP
Hs TTLL5	TRKDR—KPVASSRGRG VY---VRLYVL---LLEVNLSP
	K282 β6-7 loop (R339) R376 E517 N519
Dm TTLL5	TRKDR--KPAASSRGRG I F---LRVYVL---LLEI NLSP

767 [1)] The critical domain of the β6-7 loop is highlighted using a yellow background.

768

769

770 **Table 3) Conservation between *TTL* and *TTLL5***

771 Many critical residues of human TTL (red) are conserved in *Drosophila,* mouse, and human TTLL5
772 (Prota et al., 2013; van Dijk et al., 2007).

	R202 R222 D318 E331 N333 P336
Hs TTL	IRSW—VLRTA-----FDFM—LI EVNGAPA
	R376 R398 D504 E517 N519 P522
Dm TTLL5	LRVY---I VRLA-----FDIL----LLEI NL SPS
	R225 R247 D353 E366 N368 P371
Mm TTLL5	VRLY---LARFA-----FDVL---LLEVNL SPS
Hs TTLL5	VRLY---LARFA-----FDVL---LLEVNL SPS

773

774

775 **Table 4) Transport parameters for mitochondria in the selected region of L1 veins.**

Genotype	*Control*		*TTLL5^{E517A}*	
Direction	Plus-end	Minus-end	Plus-end	Minus-end
Number of wings (motile mito[1)])	3 (20)	3 (11)	3 (8)	3 (2)
Motile Mito[1)] (% total mito)	5.3±1.7	2.5±3.2	**1.5±1.3***	0.4±0.4
Total time (s)	92±45	100±43	98±48	64±37
Pausing (% total time)[2)]	74±14	77±15	**63±13***	61±20
Length (µm)	7.2±4.5	6.7±1.6	**12.3±5.3***	7.5±2.8
Velocity (µm/s)[3)]	0.37±0.08	0.38±0.14	0.36±0.08	0.36±0.16

776 [1)] Motile mitochondria, which showed a run distance ≥ 2 µm.

777 [2)] The pausing time ratio indicates the pausing time divided by the total duration of each motile mitochondria.

778 [3)] Mean velocity corresponds to the mean values of instant trafficking velocity. Significant differences for
779 mitochondria of plus-end transport between control and *TTLL5^{E517A}* are shown in boldface, followed by * ($p<0.05$).

780 Only two mitochondria transported toward the MT minus-end were observed in *TTLL5^{E517A}*. A comparison of the
781 minus-end transport between control and *TTLL5^{E517A}* is not warranted, and these parts are shaded in grey to
782 indicate this.

783

784 **Figure legends**

785

786 **Fig. 1 Mass spectrometry analysis of the glutamylation of the C-terminal domains of**
787 **the α-tubulin isoforms.** A) Schematic representation showing **how** the C-terminal peptides
788 of TBA1/3 can be modified by glutamic acids residues added to the side chains of E443,
789 E445, E448, and E449 in *Drosophila* ovaries. B) The C-terminal peptides containing the
790 complete primary sequence were analyzed. The structure of the different C-terminal tail
791 peptides of TBA1/3 modified by glutamylation are shown. Different combinations of Glu side
792 chain modifications were found added at positions E443, E445, E448, and E449 of TBA1/3.
793 Schemes were drawn by biorender.com.

794

795 **Fig. 2 Schematic representation of the *Drosophila TTLL5* gene, TTLL5, TTLL5^{MiEx}, and**
796 **Venus::TTLL5 proteins.** A) The *TTLL5* gene structure is based on the Flybase data for the
797 CG31108-RA transcript. The positions of the loss-of-function mutations are marked on the
798 *TTLL5* gene. Grey triangles: transposon insertions. Grey asterisks: codons targeted for
799 generating InDels and point mutations. All *TTLL5* alleles were analyzed as hemizygous
800 animals over *Df(3R)BSC679*, which removes the region of the *TTLL5* gene. B) Western blot
801 from the soluble fraction of ovarian extracts. *w* (*TTLL5^{+}/$^{+}$),* which contains two wild-type
802 copies of *TTLL5*, expressed the highest levels of TTLL5. The TTLL5 signal is strongly
803 reduced or abolished in the null mutants *TTLL5^{pBac}/$^{-}$, TTLL5^{Mi}/$^{-}$,* and *TTLL5^{MiEx}/$^{-}$* compared to
804 *w.* The hemizygous *TTLL5^{+}* ovaries (*TTLL5^{+}/$^{-}$*) expressed less TTLL5 than *w.* The signal of
805 an unspecific band (labeled with *), produced after a short exposure, was used as the
806 loading control. In the following we will refer to the genotypes as *w* for the control (*TTLL5^{+}/$^{+}$*)
807 and as *TTLL5^{allele}* for the hemizygous mutants *(TTLL5^{allele}/$^{-}$*).

808

809 **Fig. 3 *TTLL5* is required for the glutamylation of the TBA1/3 isoforms of ovarian α-**
810 **tubulin.** A) A') Sites on TBA1/3 recognized by the GT335 and 1D5 antibodies, respectively.
811 B) B') B'') The glutamylation signal produced by Western blotting with the GT335 and 1D5
812 antibodies is lower in *TTLL5^{pBac}, TTLL5^{Mi}*, and *TTLL5^{MiEx}* than in the *w* control but is restored
813 and even elevated in mutant ovaries that were rescued by *MattubGal4>Venus::TTLL5*. The
814 up-shifted bands recognized by 1D5 can be seen in the rescued *TTLL5^{pBac}* and *TTLL5^{Mi}*
815 mutants. The total tyrosinated α-tubulin levels seemed unaffected by the TTLL5 levels. B'')

816 The anti-βmono-E levels were similar between *w* control, *TTLL5*^{MiEx}, and rescue of *TTLL5*^{MiEx}.
817 α-tubulin and GAPDH served as loading controls. C) Stronger up-shifted bands were
818 observed upon *MattubGal4>Venus::TTLL5* overexpression in wild-type ovaries (anti-1D5
819 antibody). Total α-tubulin remained at similar levels in samples with excessive expression of
820 *TTLL5.* GAPDH was a loading control. D) The genotypes and rationale of the *TTLL5* alleles
821 generated by CRISPR/Cas9 are listed. The selected residues are predicted to be either
822 important for the glutamylation or tyrosination function based on the alignment shown in
823 **Tables 1** and **2**. E) Western blotting showed that the polyglutamylation signal is absent in all
824 point mutants. *w* with two copies of *TTLL5*$^{+}$ is the wild-type control and *TTLL5*$^{K282\ indel3}$ is a
825 hemizygous additional control in which the neighbors of K282, T280R281 were replaced by
826 K280G281. Relative 1D5 signal levels decreased slightly in the hemizygous samples with
827 only one *TTLL5* copy. All *TTLL5* alleles were analyzed as hemizygous animals over
828 *Df(3R)BSC679*, which removes the region of the *TTLL5* gene. The genotypes for rescues
829 were *MattubGal4>UAS-Venus::TTLL5;TTLL5*^{alleles}*/Df(3R)BSC679.* The genotype for
830 *Venus::TTLL5* overexpression was *MattubGal4>UAS-Venus::TTLL5.*

831

832 **Fig. 4 Effect of *TTLL5* on Staufen posterior localization refinement in oocytes.**

833 A) A') Confocal micrographs showing stage 10B oocytes of *w* controls and *TTLL5*^{pBac},
834 *TTLL5*^{Mi}, and *TTLL5*^{MiEx} mutants. A'') Confocal micrographs showing stage 10B oocytes of
835 *TTLL5*^{pBac}, *TTLL5*^{Mi}, and *TTLL5*^{MiEx} mutants rescued with *Mattub4>UASP-Venus::TTLL5*.
836 Anti-Staufen is shown in green, anti-GFP in red, and Hochest in blue. A''') Quantification of
837 the Staufen crescent length along the posterior cortex based on A, A' and A''. B) Confocal
838 micrographs showing stage 10B oocytes of *w* controls, *TTLL5*^{E517A}, *TTLL5*^{P522A}, and
839 *TTLL5*^{R339A} mutants. B') Quantification of Staufen's crescent length along the posterior cortex
840 based on B). C) Confocal micrographs showing previtellogenic egg chambers of *w* controls,
841 *TTLL5*^{E517A}, *TTLL5*^{P522A}, *TTLL5*^{R339A}, and *TTLL5*^{pBac} mutants. BicD protein, *BicD* and *osk*
842 mRNA are shown in red, Staufen protein in green, and Hochest in blue. The white
843 arrowheads in the *BicD* images point out the localized *BicD* mRNA in oocytes. D) The BicD
844 levels remained unchanged between *w* control, *TTLL5*^{MiEx}, and *TTLL5*^{MiEx} rescued by
845 *Mattub4>Venus::TTLL5.* GAPDH served as the loading control. *** $p<0.005$; ** <0.01. Scale
846 Bars: 25 μm. All *TTLL5* alleles were hemizygous over *Df(3R)BSC679*. The genotypes for
847 rescued animals were *MattubGal4/UAS-Venus::TTLL5; TTLL5* ^{alleles}*/Df(3R)BSC679.*

848

849 **Fig. 5 Role of *TTLL5* in ooplasmic streaming.** A) KHC levels remained unchanged
850 between *w* control, *TTLL5*^{MiEx}, and *TTLL5*^{MiEx} rescued by *Mattub4>Venus::TTLL5.* GAPDH
851 served as the loading control. B) Example picture of a stage 10B oocyte used for particle
852 flow measurements based on time-lapse movies of ooplasmic streaming (Mov.S1-S4). Scale
853 Bar: 25 µm. C) 100-200 particles were selected along the cortex line from two sides of each
854 ooplasm to determine the mean velocities of the particles from the different genotypes. One
855 stage 10B oocyte was chosen randomly for velocity quantification for each fly. The fly
856 numbers for *w* control, *TTLL5*^{MiEx} mutant, *TTLL5*^{E517A} mutant, and *UASP-Venus::TTLL5*
857 transgene rescuing the *TTLL5*^{MiEx} mutant were 7, 9, 5, and 5, respectively. No significant
858 changes in particle velocity were found between different genotypes. D) Representative
859 kymographs of particles in oocytes of a *w* control, a *TTLL5*^{MiEx} mutant, the *TTLL5*^{E517A}
860 mutant, and the *TTLL5*^{MiEx} mutant rescued by overexpression of the *UASP-Venus::TTLL5*
861 transgene. Kymographs were generated along a line (the yellow line in B) close to the cortex
862 on each side of the ooplasm from 3 min time-lapse movies. Representative kymographs
863 showed that the particles flowed along the cortex in both control and *Venus::TTLL5* rescue.
864 In contrast, the moving particles revealed different flow patterns if TTLL5 activity was low.
865 Genotypes for *TTLL5*^{MiEx} and *TTLL5*^{E517A} were *TTLL5*^{MiEx}*/Df(3R)BSC679* and
866 *TTLL5*^{E517A}*/Df(3R)BSC679*, respectively. The genotype of the rescued flies was
867 *MattubGal4/UAS-Venus::TTLL5; TTLL5*^{MiEx}*/Df(3R)BSC679.*

868

869 **Fig. 6 Effect of *TTLL5* on mitochondria transport in the wing nerve.** A) In head and wing
870 extracts, the relative glutamylation signal of 1D5 is lower in *TTLL5*^{E517A} (genotype: *ApplGal4;*
871 *UAS-Mito::GFP; TTLL5*^{E517A}*/Df(3R)BSC679*) than in the control (genotype: *ApplGal4;UAS-*
872 *Mito::GFP;+/Df(3R)BSC679*). B) Cartoon of the *Drosophila* wing showing the L1 and L3 vein
873 and the neuron-rich regions analyzed for tracking mitochondria (red and green boxes). C)
874 Representative still image of GFP-labelled mitochondria in axons of the L1 and L3 vein (from
875 **Mov. S5** and **Mov. S6**, respectively) of both control and *TTLL5*^{E517A} wings. Transported
876 mitochondria (run distance ≥ 2 µm) were manually labeled with the Fiji MTrackJ plugin.
877 Some circles only mark a mitochondrial signal that appeared in another time frame. Scale
878 Bar: 10 µm. D) Quantification of the fraction of transported mitochondria. Note that in control
879 wings, a much higher fraction of mitochondria is transported in the L3 vein than in L1. The
880 results from L1 show a dramatic decrease of motile mitochondria in the *TTLL5*^{E517A} mutant.
881 In the L3 vein, no transported mitochondria were found in the *TTLL5*^{E517A} mutant. The total
882 particles (indicated by "n") with a diameter from 0.1µm-1.6µm were analyzed by Fiji from the
883 signals of a representative still images from three wings for each genotype. The motile

884 mitochondria ratio indicates the number of transported mitochondria divided by total
885 mitochondria particles. E) Scheme of the transport behavior of the mitochondria in the wing
886 neuron. The start of a run was either considered the time when a motile particle began to
887 move from a stationary position or entered into the focal plane. Particles were defined as
888 “trafficking” when their instant velocity was ≥ 0.2 μm/s, and they were considered as
889 “pausing” when they moved at less than 0.2 μm/s but later resumed their movement. As the
890 stop of a run we considered particles that entirely terminated or moved out of the focal plane.
891 For each run, the total run distance of more than 2 μm was considered as “transported or
892 motile mitochondria”. *** $p<0.005$; * <0.05. Schemes were drawn by biorender.com.

Fig. 1

A

α-tubulin isoforms in *Drosophila* ovaries

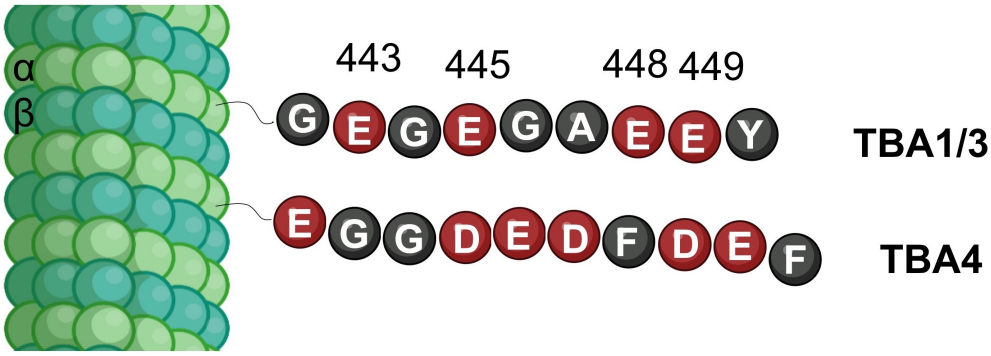

E-residues were found added at the TBA1/3 positions E443, E445, E448 and E449.

B

Glutamylation on Glu residues in the C-terminal domain of TBA1/3

GEGEGAEEY E	GEGEGAEEY E	GEGEGAEEY E	GEGEGAEEY E
GEGEGAEEY EE	GEGEGAEEY EE	GEGEGAEEY EE	GEGEGAEEY EE
GEGEGAEEY EEE	GEGEGAEEY EEE	GEGEGAEEY EEE	GEGEGAEEY EEE
GEGEGAEEY E E	GEGEGAEEY E EE	GEGEGAEEY E E	GEGEGAEEY E EE
GEGEGAEEY EEE	GEGEGAEEY E E E		

Fig. 2

A

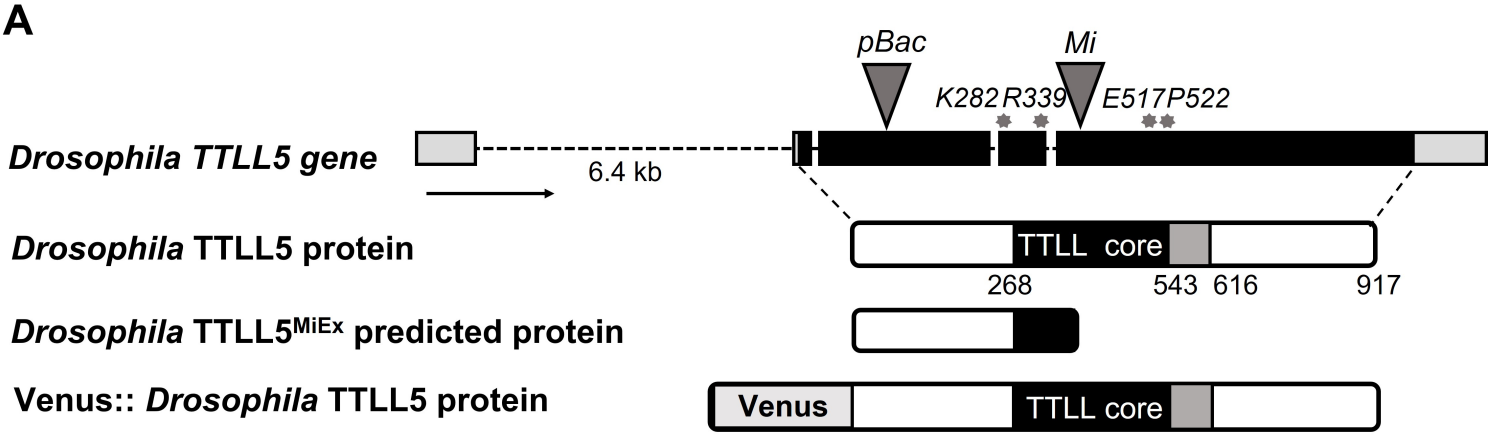
pBac
Mi
K282 R339
E517 P522
Drosophila TTLL5 gene
6.4 kb
Drosophila TTLL5 protein
TTLL core
268
543
616
917
Drosophila TTLL5MiEx predicted protein
Venus:: Drosophila TTLL5 protein
Venus
TTLL core

B

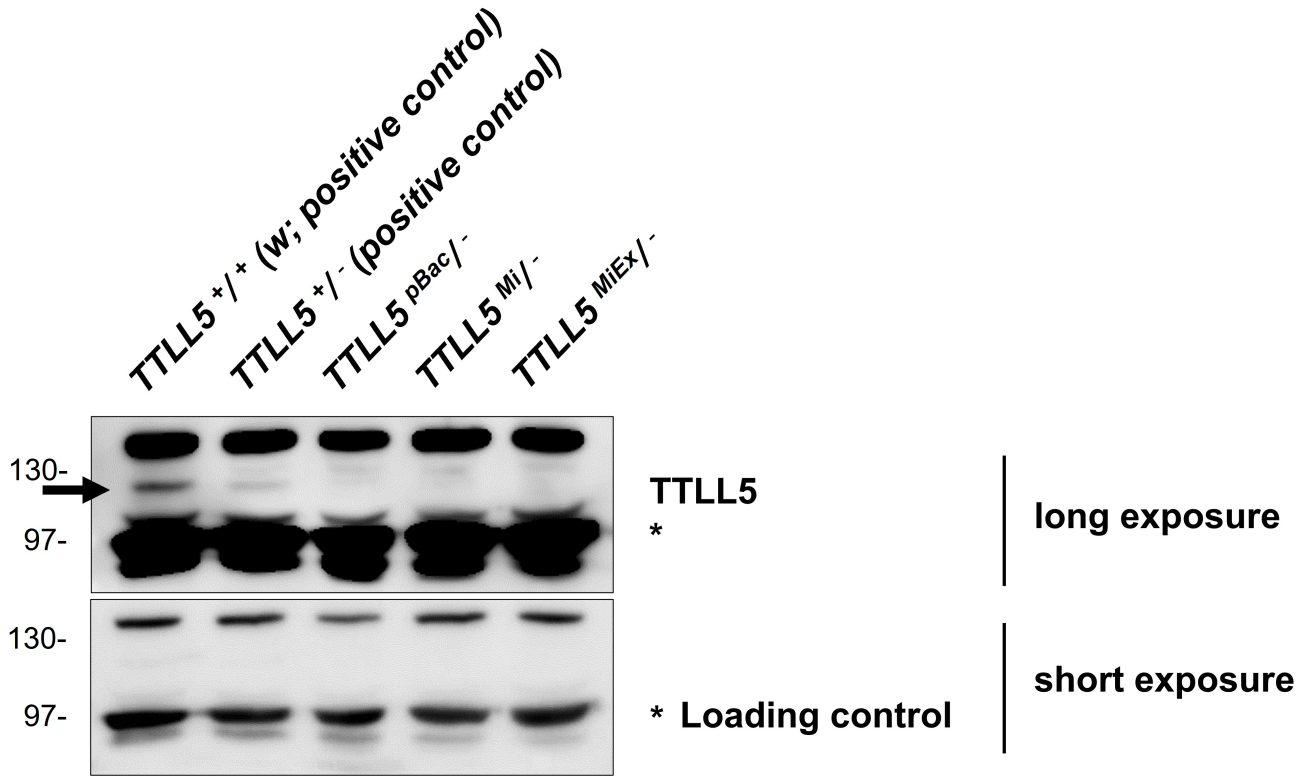
TTLL5 +/+ (w; positive control)
TTLL5 +/- (positive control)
TTLL5 pBac/-
TTLL5 Mi/-
TTLL5 MiEx/-
130-
97-
TTLL5
*
long exposure
130-
97-
* Loading control
short exposure

Fig. 3

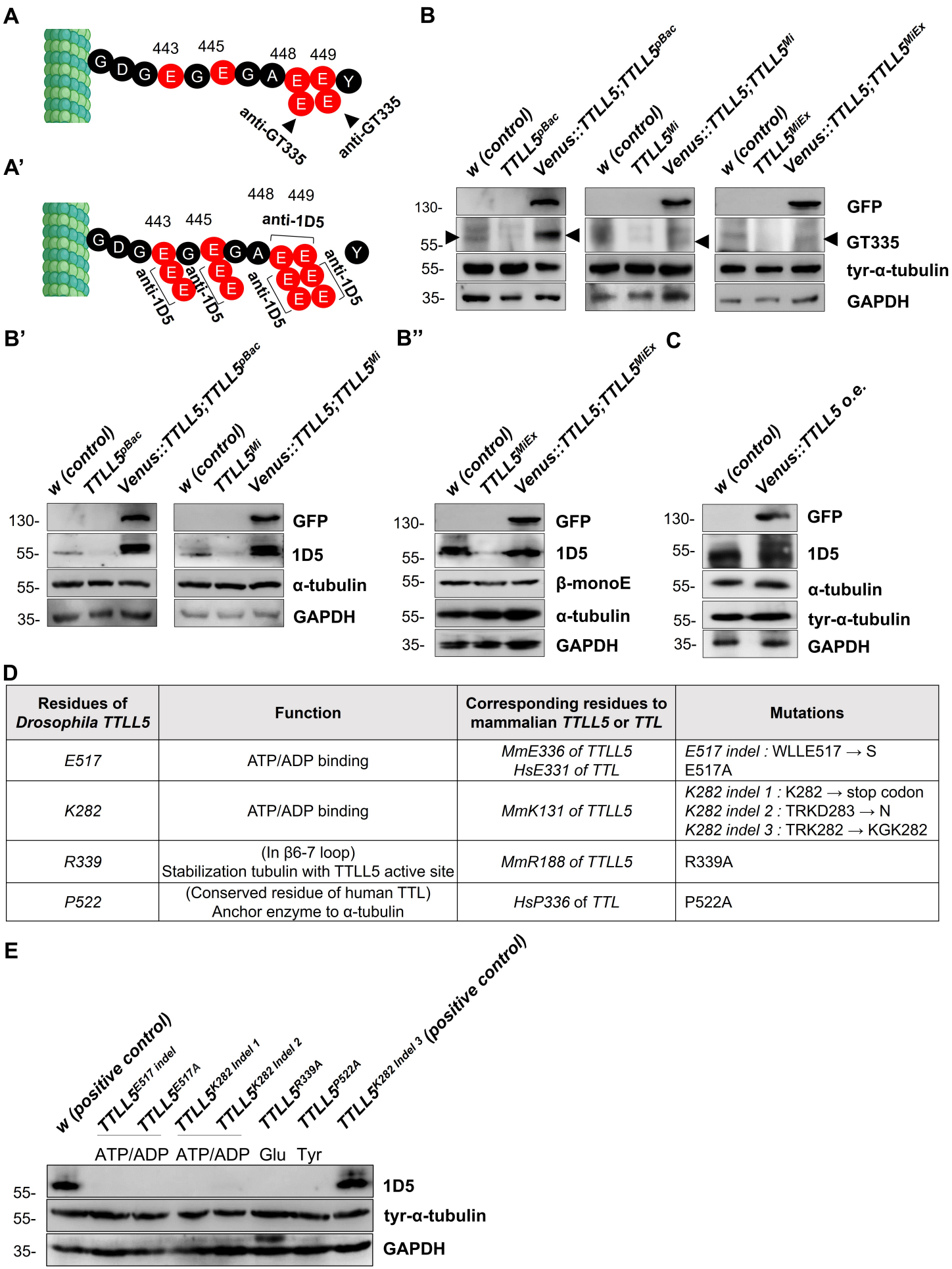

Residues of *Drosophila TTLL5*	Function	Corresponding residues to mammalian *TTLL5* or *TTL*	Mutations
E517	ATP/ADP binding	*MmE336 of TTLL5* *HsE331 of TTL*	*E517 indel :* WLLE517 → S E517A
K282	ATP/ADP binding	*MmK131 of TTLL5*	*K282 indel 1 :* K282 → stop codon *K282 indel 2 :* TRKD283 → N *K282 indel 3 :* TRK282 → KGK282
R339	(In β6-7 loop) Stabilization tubulin with TTLL5 active site	*MmR188 of TTLL5*	R339A
P522	(Conserved residue of human TTL) Anchor enzyme to α-tubulin	*HsP336* of *TTL*	P522A

Fig. 4

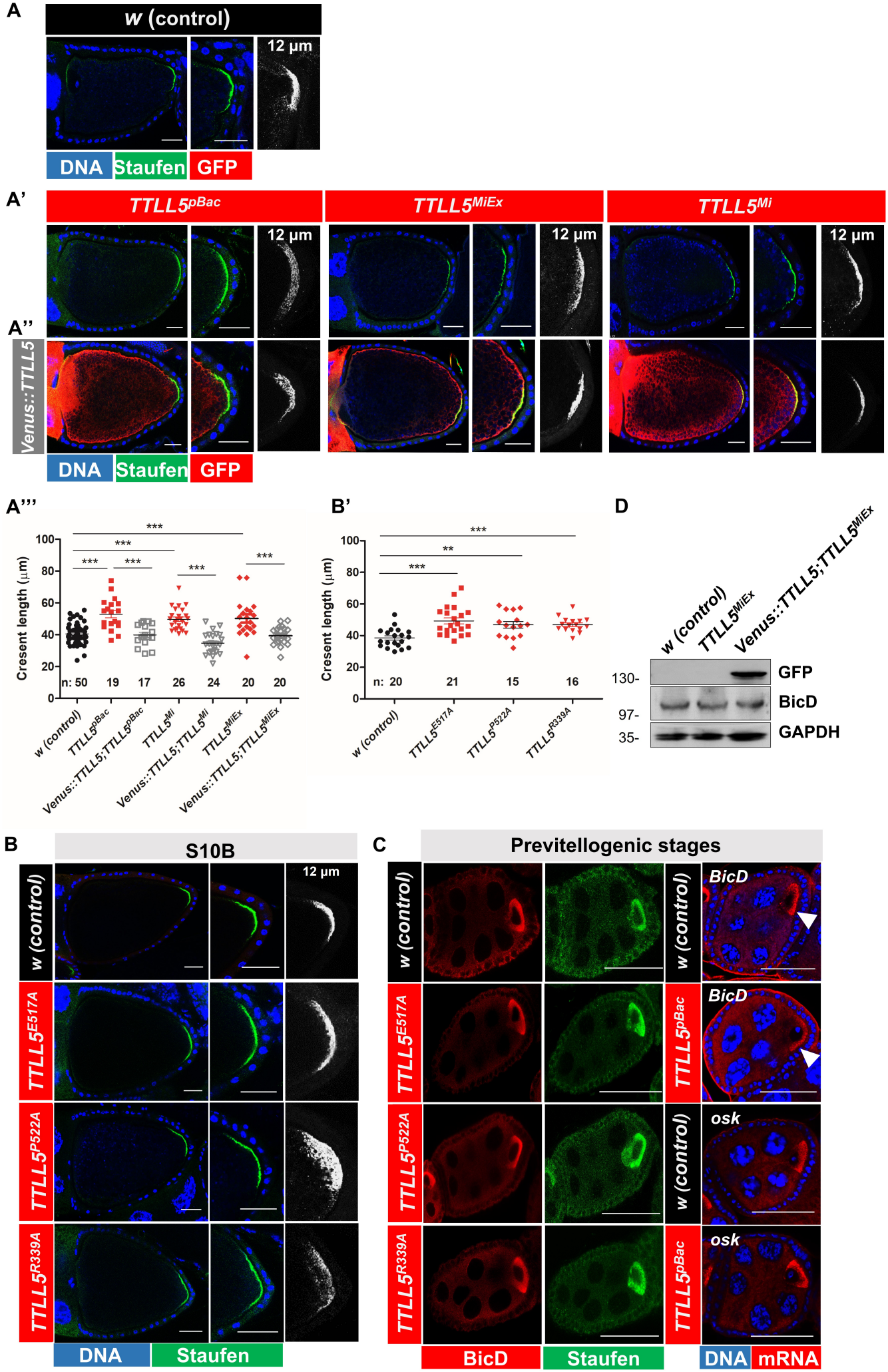
A
w (control)
12 µm
DNA
Staufen
GFP
A'
TTLL5pBac
TTLL5MiEx
TTLL5Mi
12 µm
A''
Venus::TTLL5
DNA
Staufen
GFP
A'''
Cresent length (µm)
n: 50
19
17
26
24
20
20
w (control)
TTLL5pBac
Venus::TTLL5;TTLL5pBac
TTLL5Mi
Venus::TTLL5;TTLL5Mi
TTLL5MiEx
Venus::TTLL5;TTLL5MiEx
B'
Cresent length (µm)
n: 20
21
15
16
w (control)
TTLL5E517A
TTLL5P522A
TTLL5R339A
D
w (control)
TTLL5MiEx
Venus::TTLL5;TTLL5MiEx
130-
97-
35-
GFP
BicD
GAPDH
B
S10B
w (control)
TTLL5E517A
TTLL5P522A
TTLL5R339A
12 µm
DNA
Staufen
C
Previtellogenic stages
w (control)
TTLL5E517A
TTLL5P522A
TTLL5R339A
BicD
TTLL5pBac
osk
BicD
Staufen
DNA
mRNA

Fig. 5

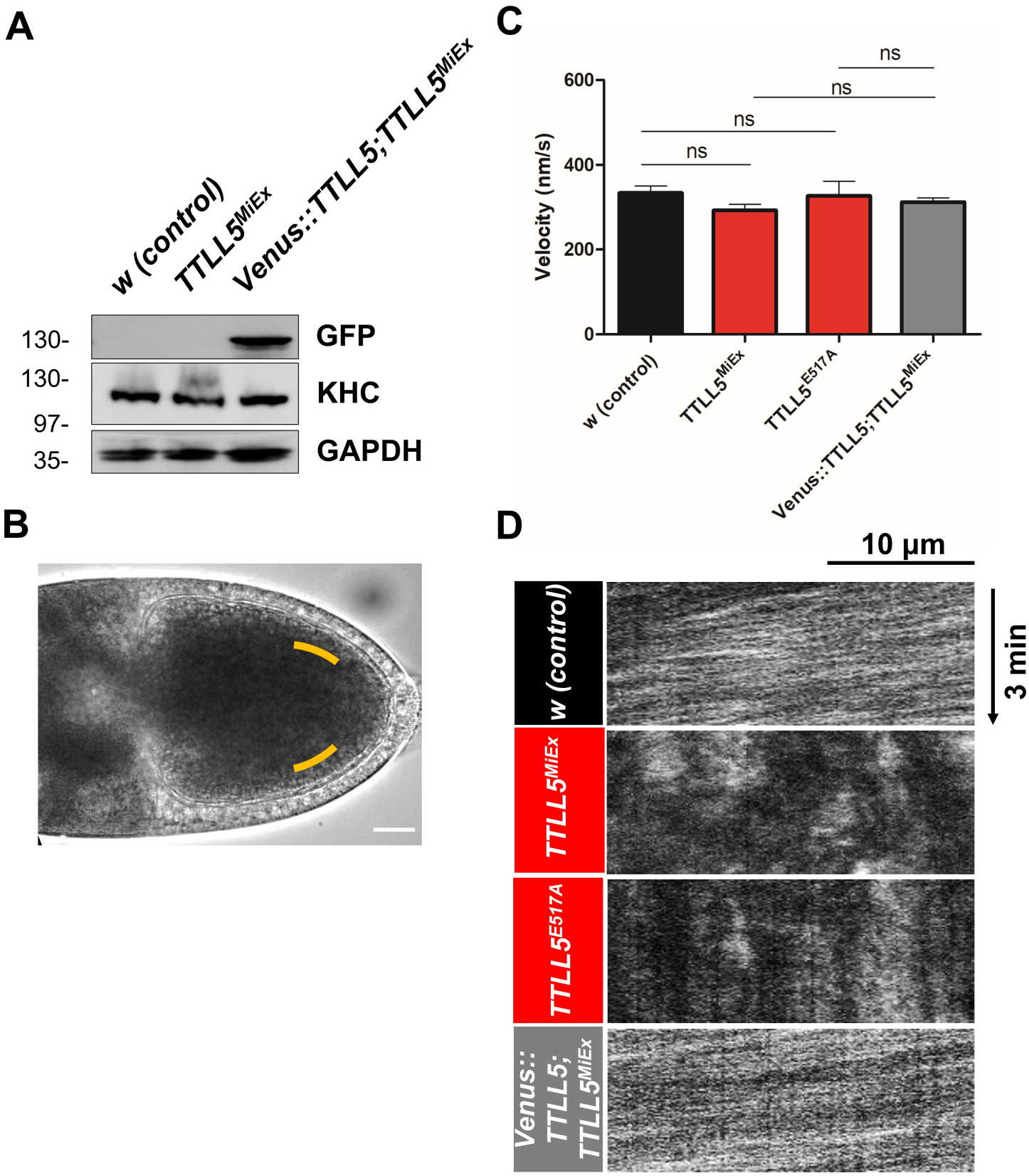
A
w (control)
TTLL5MiEx
Venus::TTLL5;TTLL5MiEx
130-
130-
97-
35-
GFP
KHC
GAPDH
B
C
Velocity (nm/s)
600
400
200
0
ns
ns
ns
ns
w (control)
TTLL5MiEx
TTLL5E517A
Venus::TTLL5;TTLL5MiEx
D
10 µm
3 min
w (control)
TTLL5MiEx
TTLL5E517A
Venus::
TTLL5;
TTLL5MiEx

Fig. 6

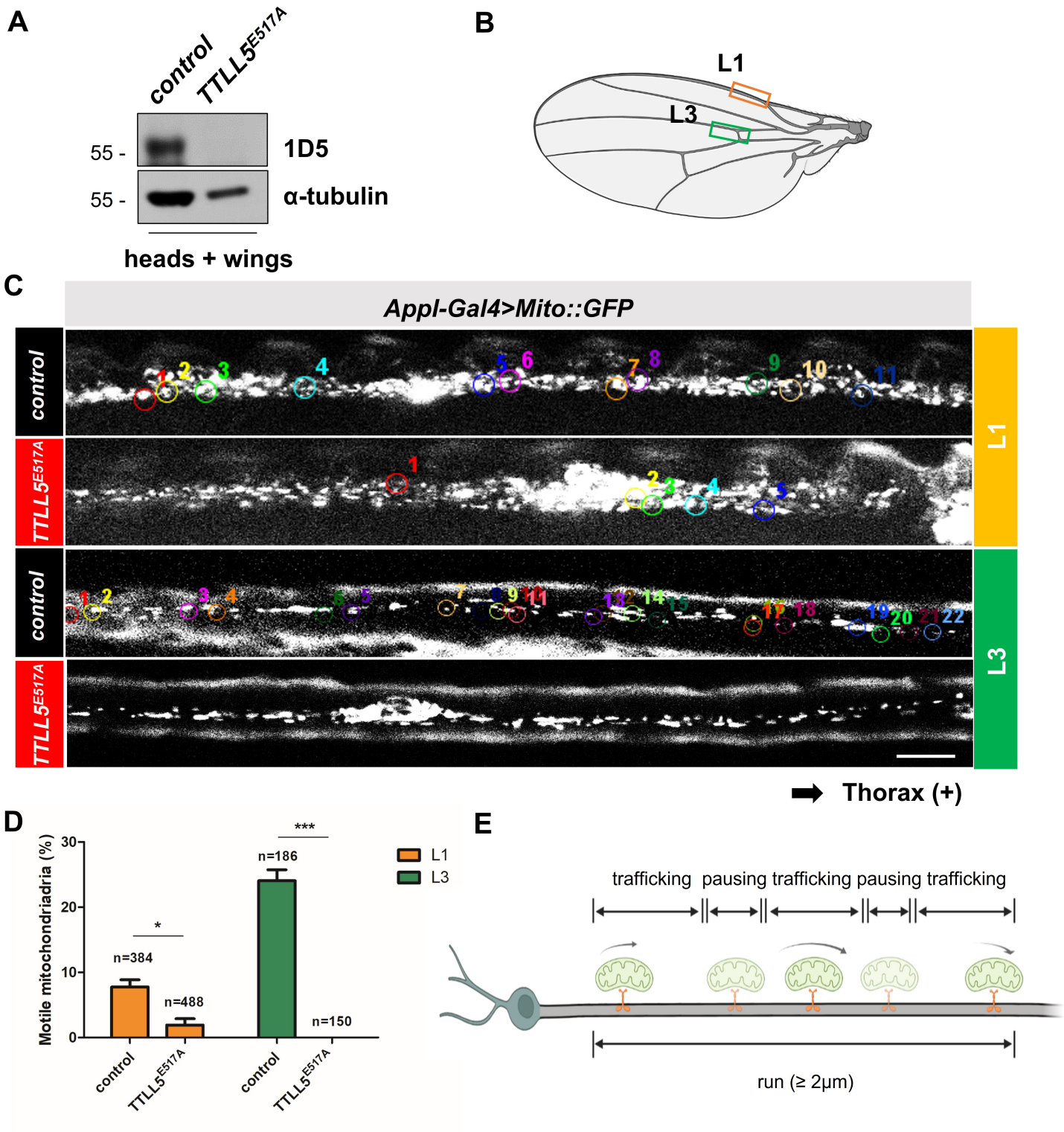
A
control
TTLL5E517A
55 -
55 -
1D5
α-tubulin
heads + wings
B
L1
L3
C
Appl-Gal4>Mito::GFP
control
TTLL5E517A
control
TTLL5E517A
L1
L3
Thorax (+)
D
Motile mitochondriadria (%)
30
20
10
0
*
***
n=384
n=488
n=186
n=150
control
TTLL5E517A
control
TTLL5E517A
L1
L3
E
trafficking
pausing
trafficking
pausing
trafficking
run (≥ 2μm)